DESIGN OF AN ACTIVELY COOLED GRID SYSTEM TO IMPROVE EFFICIENCY IN INERTIAL ELECTROSTATIC CONFINEMENT FUSION REACTORS

ANDREW SELTZMAN

GEORGIA INSTITUTE OF TECHNOLOGY

DEPARTMENT OF PHYSICS

ABSTRACT

Traditional inertial electrostatic confinement (IEC) fusion reactor designs utilize an ion accelerating grid fabricated out of a refractory metal capable of operating at high temperatures to radiate off heat imparted by ion-grid collisions. Unfortunately, the high gird temperature allows for a substantial thermionic electron emission current, requiring a high power draw and significantly reducing reactor efficiency. Further, electrons emitted from the grid are accelerated into the reactor shell where they generate a significant amount of bremsstrahlung x-rays requiring additional shielding and increasing system size and weight.

Presented is a novel modification to the traditional implementation of an IEC fusion reactor, designed to improve operating efficiency by reducing electron emission from the grid. A liquid cooled grid design is utilized to reduce thermionic electron emission, allowing for higher plasma densities, and greater input power while improving system efficiency and reducing x-ray output. The resulting low grid temperatures substantially reduce thermionic electron emission and greatly improve reactor efficiency by reducing current draw from the central grid. The reduction of thermionic electron emission will eliminate the majority of bremsstrahlung x-ray generation thereby reducing shielding requirements.

By measuring the heat deposited into the coolant, the grid cooling system may also be used as a diagnostic tool to study the physics involved in IEC reactors. In this manner, grid transparency may be directly measured as a function of ion bombardment heating. By modifying the confinement scheme of the reactor and subsequently evaluating the energy flux to the grid through ion collisions, greater energy and particle confinement times may be obtained.

Table of Contents

List of Figures

List of Tables

CHAPTER 1
INTRODUCTION

Inertial Electrostatic Confinement Fusion Overview

Inertial electrostatic confinement (IEC) is a unique fusion reactor concept in which deuterium ions are accelerated toward a focal point by an electric field resulting in fusion. An IEC fusion reactor consists of a spherical accelerating grid centered within a spherical vacuum chamber. The accelerating grid is traditionally constructed out of overlapping rings arranged to form a sphere that maintains a high degree of transparency. Optionally, an ion source is located near the edge of the vacuum chamber, generating a source of positively charged deuterium ions. When the accelerating grid is biased at a negative potential with respect to the vacuum chamber, positively charged deuterium ions are accelerated towards the grid; however, due to the high degree of transparency, the majority of the ions pass through the surface of the grid with out colliding with it. (Figure 1-1)

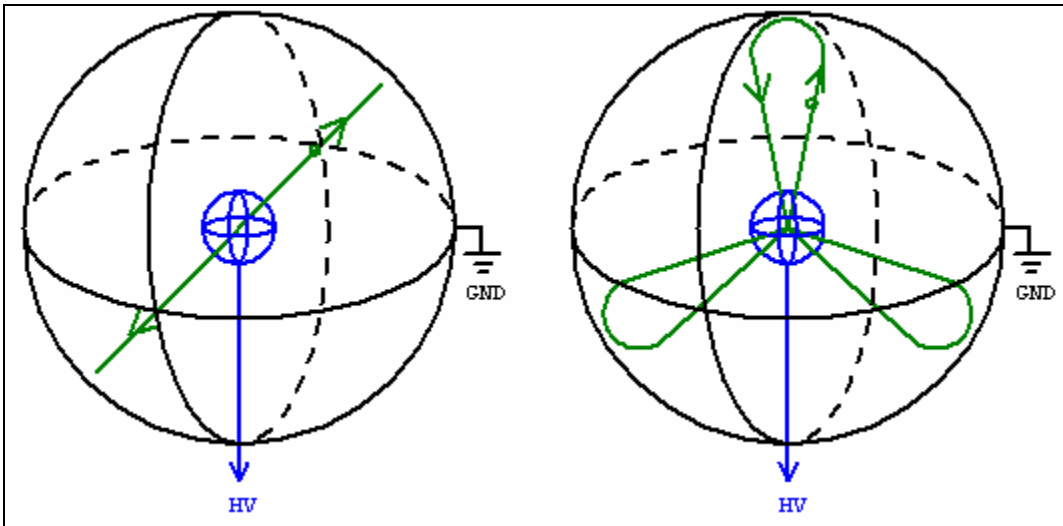

Figure 1-1. Ideal and realistic ion trajectory.

Once inside the grid, the ions are shielded from the electric field and collide at the focal point due to their inertia. As the ions converge on the focal point, the density of the deuterium plasma increases geometrically, increasing

the possibility of an ion – ion collision. When the deuterium ions collide at the focal point, a small fraction will fuse with other deuterium ions (D-D fusion) while the majority will either scatter off other deuterium ions or pass through without collision.

Non-fusing ions will then travel outward, passing through the grid into the electric field, where they will decelerate as they travel outward and then accelerate back towards the center. In this manner the ions will repeatedly oscillate through the focal point, thereby increasing the probability for a given ion to fuse with another. The ions will continue to oscillate until they are neutralized by a collision with the grid, chamber or a free electron. At this point the deuterium atom will be either re-ionized or pumped out of the reactor by the vacuum system.

Applications of IEC Fusion Reactors

The simple nature of the vacuum chamber – grid electrostatic confinement design allows the IEC fusion reactor to be used as a portable source for high energy neutrons and protons generated by the D – D fusion reaction. Unlike an isotope based neutron source, where an alpha decaying isotope power is permanently mixed with a beryllium power inside a sealed container, IEC neutron sources contain no radioactive material, thereby eliminating the need for an isotope license. Further, IEC neutron sources can be shut down, allowing for easy storage without shielding. Due to the portability, low cost, and high performance, IEC fusion reactors are beginning to replace isotope neutron sources in certain diagnostic and analytical applications.

High energy protons produced by the D – D fusion reaction are used for the generation of medical isotopes used in PET scans, while neutrons may be used in industrial and analytical applications. Neutrons can be used in neutron activation analysis, where short lived isotopes are generated, and the energy of their decay products is analyzed, allowing identification of the material in question. Neutron sources may also be used in the detection of fissile material in nuclear weapons by prompt gamma generation, or in the detection of explosives

and non-metallic land mines by backscattering neutrons off of hydrogen and nitrogen rich materials.

CHAPTER 2
LITRATURE REVIEW

IEC Reactor Design Overview

Inertial Electrostatic Confinement (IEC) is a unique fusion reactor concept in which deuterium ions are electrostatically accelerated in a spherically convergent manner and subsequently inertially confined by their momentum as they collide at a focal point resulting in their fusion. IEC fusion was initially developed by Philo T. Farnsworth in the 1960's utilizing RF fields for ion acceleration and later modified by Dr. Robert Hirsch and Gene Meeks allowing for ion acceleration with electrostatic fields by the use of a spherical ion accelerating grid.

A Hirsch-Meeks type IEC fusion reactor typically consists of a spherical inner grid that is held at a negative potential in the order of 100kV and surrounded by a grounded spherical vacuum envelope. Traditionally in the simplest of the Hirsch-Meeks designs, the inner grid emits electrons that are electrostatically accelerated towards the vacuum envelope, subsequently ionizing neutral deuterium atoms in the reactor. The ionized deuterium is then accelerated towards the center grid by the electrostatic field. Since the projected area of the grid only occupies a small solid angle, the majority of the accelerated ions pass through the grid structure and collide at a focal point where the fusion takes place. (Dietrich)

Since Earnshaw's theorem forbids the creation of a potential minimum in free space, it is not possible to electrostatically confine the deuterium ions at the focal point; however they may be inertially confined by their momentum once they pass the surface of the accelerating grid. In the limit where the accelerating grid is much smaller than the vacuum envelope, the monopole term of the multipole expansion is dominant, and the electrostatic field closely approximates a spherically symmetric source over the majority of the acceleration path of a

given ion, generating a sharp focus and increasing plasma density limited only by space charge repulsion, thereby leading to a large fusion rate. In this manner a spherical source can be well approximated by an accelerating grid constructed out of three perpendicular rings if the aspect ratio of the grid diameter to the vacuum chamber diameter is small.

Problems with Traditional IEC Fusion Designs

In a traditional IEC fusion reactor the maximum input potential to the central grid, and therefore the maximum fusion rate of the reactor, is limited by grid heating and a condition called thermionic runaway. (Piefer) Above a certain input power threshold and neutral species pressure within the reactor, any increase in grid temperature by ion bombardment increases the grid's thermionic electron emission rate leading to greater neutral ionization rates within the reactor, continuously increasing ion bombardment heating until the grid melts. The central grid of an IEC fusion device may still melt even if a thermionic runaway does not occur, if ion bombardment heating can raise the grid temperature above its melting point. Further, ion bombardment heating causes increased sputtering and sublimation rates, leading to plasma impurities, grid erosion, and metal deposition on critical components such as ceramic feedthroughs, insulators and view ports. Further, thermionically emitted electrons are accelerated outward and collide with the vacuum envelope generating a significant amount of bremsstrahlung x-rays capable of damaging CCD cameras and requiring shielding when operating at higher acceleration potentials.

Several conventional approaches currently exist to address melting of the central grid, including the use of high melting point refractory metals such as tungsten for grid construction. While designing a reactor with these modifications does permit the central grid to withstand ion bombardment, these solutions create further problems that contribute significant energy losses and decrease neutron production efficiency.

The construction of a grid with a refractory material allows the grid to operate at higher temperatures increasing the radiative heat dissipation rate by Planck's law; however, the higher operating temperature increases the thermionic electron

emission (Figure 1-2) rate requiring a significant increase in power supply current, and greatly decreasing reactor efficiency.

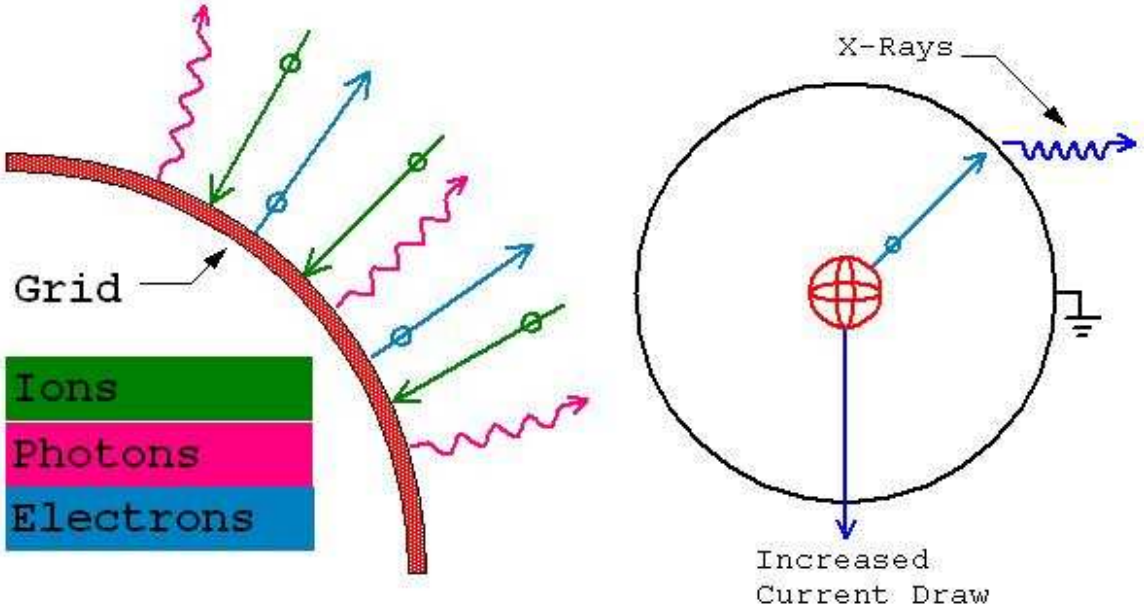

Figure 1-2. Thermionic electron emission.

Research Goal

The research presented in this thesis will solve the problem of grid heating due to ion bombardment by implementing an actively cooled grid system. The accelerating grid is constructed out of a continuous length of 1/16” OD stainless steel tubing through which a chilled coolant is pumped thereby maintaining the grid at a low temperature. The low grid temperature eliminates thermionic electron emission and improves reactor efficiency by reducing current draw. Further, by allowing direct measurement of ion bombardment heating to the grid, the fundamental physics of the IEC device may be better understood by allowing determination of grid transparency.

Modifications Implemented in the Mark 3 IEC Fusion Reactor

The Mark 3 IEC fusion reactor was constructed for the purpose of researching the application of an actively cooled grid design to significantly

reduce both power draw and x-ray emission by virtually eliminating thermionic emission current from the central grid, thereby increasing reactor efficiency.

No previously constructed IEC fusion system has used an actively cooled grid for several reasons, primarily the contact of the cooling medium with the high voltage grid. This requires the entire primary cooling loop to float at grid potential, often as high as 100 kV, or the use of a non-conducting cooling medium. Further this requires the use of a high voltage dual liquid feed through, a component not commonly manufactured.

The implementation of an actively cooled grid system will significantly increase operation power and boost neutron fluxes by allowing higher input voltages. Further, by reducing thermionic emission through cooling the central grid, a lower current, higher voltage power supply can be used, increasing ion energies and reducing construction cost. The decrease in thermionic emission will virtually eliminate the generation of bremsstrahlung x-rays generated by the reactor, reducing the amount of radiation shielding required.

The Mark 3 reactor further improves plasma energy and density by utilizing a set of four ion injectors to inject ionized deuterium beams into the reactor. (Takamatsu) A novel type of compact ion injector utilizing RF ionization at the electron cyclotron resonance frequency (ECRF) was therefore constructed to provide fuel for the reactor. (Dougar-Jabon) The implemented ECRF injector design differs from conventional ion injector designs in that the ECRF antenna coil is biased at a high positive potential to provide the ion extraction field and is surrounded by an axial ceramic insulation shroud, rather then the extractor cone being biased at a negative potential as in conventional designs. (Hirsch) To conserve power and allow for a compact design the ion injector is constructed with permanent magnets to provide the axial field. The ion injector has been designed fit within a 2.75” conflat half nipple to allow the construction of a compact system.

The deuterium beams emitted from the ion injectors are focused through the open areas of the accelerating grid and are aligned to collide at the focal point, resulting in a sharper plasma focus then in a reactor with passive ionization

due to electron emission from the central grid. The use of ion injectors allows higher energy collisions by imparting additional energy above the electrostatic well potential of the grid to deuterium ions. Due to the exponential dependence of the deuterium cross section on ion energy, any increase will significantly increase neutron output.

By implementing the above mentioned improvements to the IEC fusion reactor concept, the resulting design can obtain higher neutron output levels and efficiencies than is presently capable with conventional designs while maintaining a high degree of portability.

CHAPTER 3
REACTOR DESIGN

IEC Reactor Design Overview

The Mark 3 IEC fusion reactor (Figure 3-1, Figure 3-2) is designed to be a compact, modular test bed for IEC fusion related components, in particular the cooled grid assembly. The reactor consists of several major subsystems including a cooled grid and the associated grid cooling system, a heavy water elecrolyzer for deuterim production, a gas handling system for deuterium storage and metering, an ECRF ion injector system, a high voltage power supply, a vacuum system and a computer control system allowing automatic monitoring and data logging. These key components, in particular the grid assembly and grid cooling system are described herein.

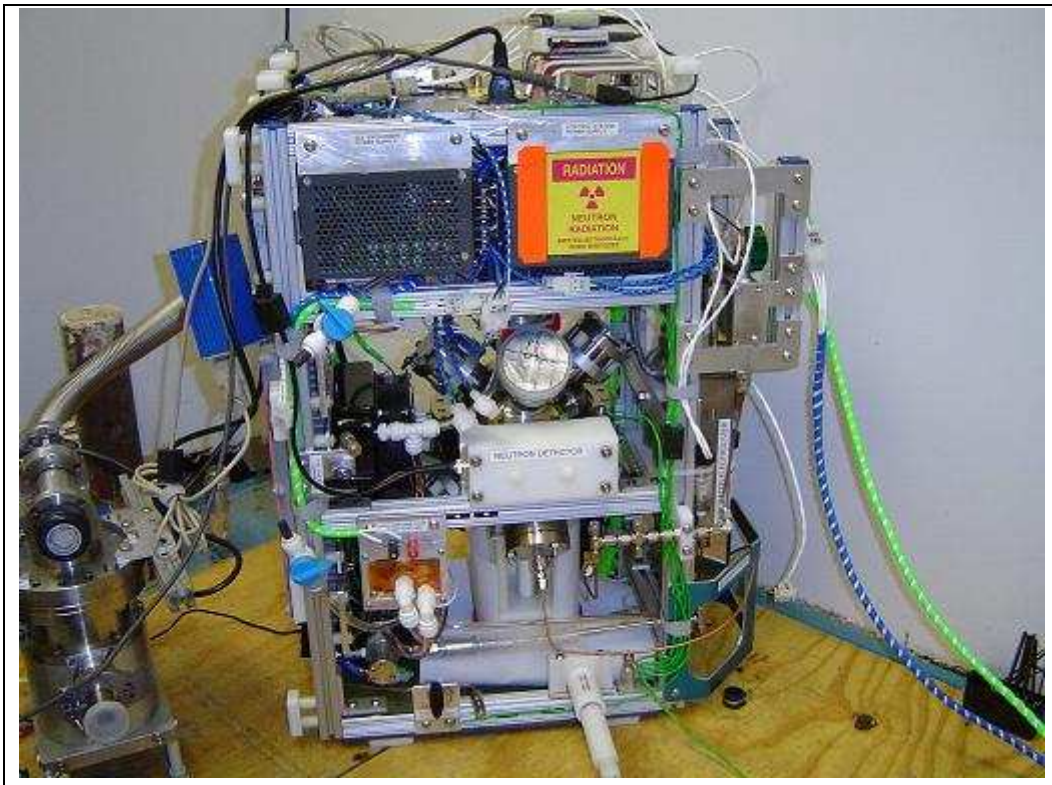

Figure 3-1. Reactor setup.

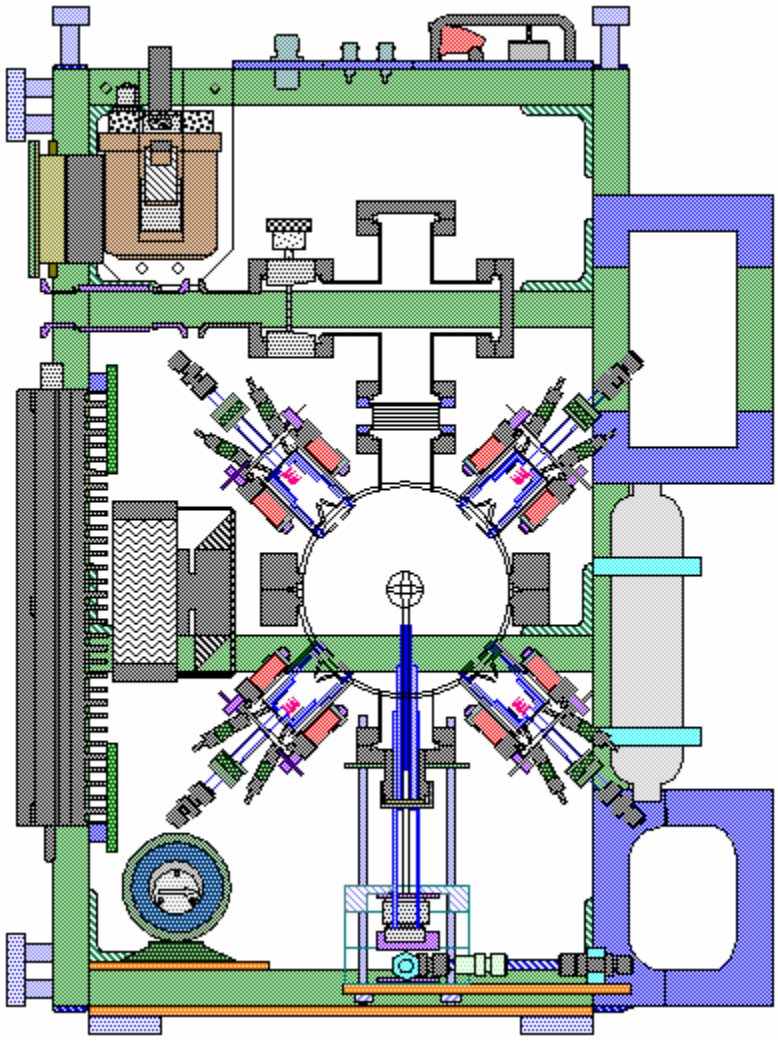

Figure 3-2. Mark 3 reactor design.

Liquid Cooled Ion Accelerating Grid

The cooled central grid system (Figure 3-3) consists of a continuous length of 1/16” OD stainless steel tube formed into three perpendicular rings of 1" in diameter and centered within the reactor envelope. The grid assembly is constructed to allow the flow of a non-conductive coolant from a grounded cooling system to pass into the grid system which is biased at -50kV by use of insulating ceramic breaks. Further the system in designed to minimize the amount of exposed high voltage components and provide a good vacuum seal while maintaining a high degree of serviceability and reliability.

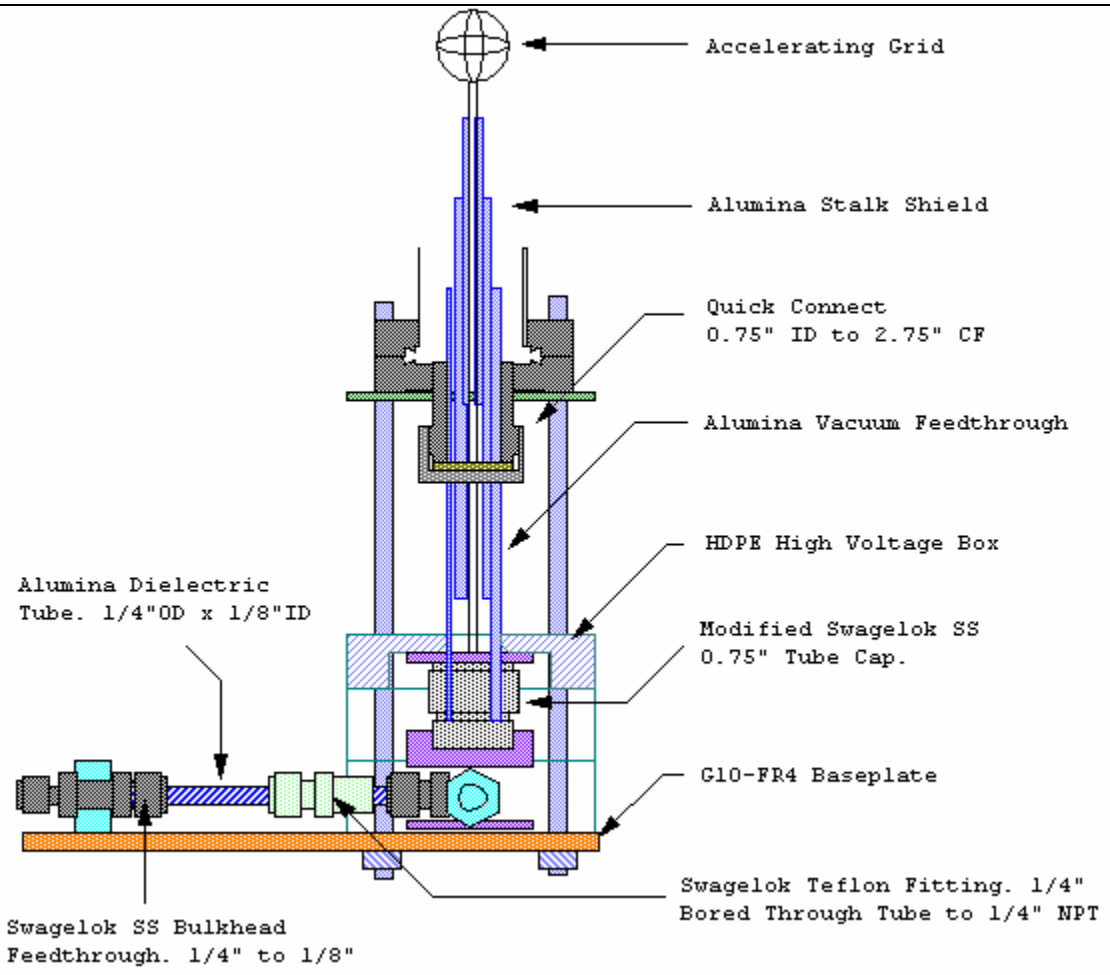

Figure 3-3. Cooled grid assembly.

The upper grid assembly (Figure 3-4) consists of a conflat quick connect seal allowing a 0.75" OD alumina ceramic rod to pass through the vacuum envelope of the reactor while maintaining a high vacuum seal. The quick connect is separated from the top of the high voltage box by a series of 1/2" OD 1/4"ID nylon spacers held in place by a 1/4"-20 threaded nylon rod. By varying the number of nylon spacers, the cooled grid may be accurately centered within the reactor. The top of the high voltage box assembly incorporates an o-ring seal to further increase insulation and help prevent condensation on cooled components by sealing out moisture.

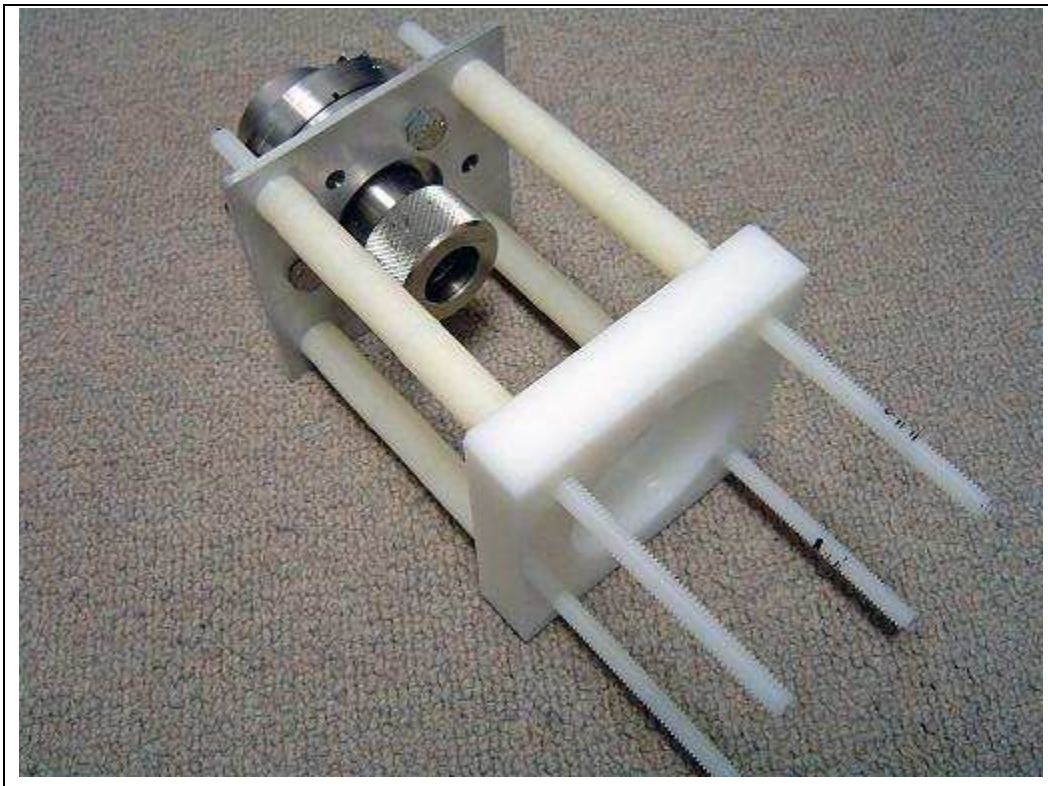

Figure 3-4. Upper grid assembly.

The lower grid assembly (Figure 3-5) consists of the base of the high voltage box including a G10-FR4 fiberglass base plate as well as the high voltage power connector and the coolant feedthroughs. Coolant is pumped through the grid assembly from a grounded pumping system that must be separated from the high voltage components of the grid, therefore a pair of 1/4" OD 1/8" ID alumina ceramic insulators were incorporated into the grid design to

provide the required high voltage insulation. The coolant is fed through a pair of 1/8" to 1/4" bulkhead feedthoughs that connect to the alumina tubes with nylon ferrules. The feedthroughs are mounted on a fiberglass base plate to prevent excessive force from being applied to the ceramic tubes. The ceramic tubes enter the high voltage box through a pair of bored through teflon stagelok fittings that secure the tubes in place, and provide additional insulation. A power connector constructed by mounting a banana jack within a 3/8" stagelok tube fitting is mounted on the side of the HV box allowing for a power connection to the high voltage supply.

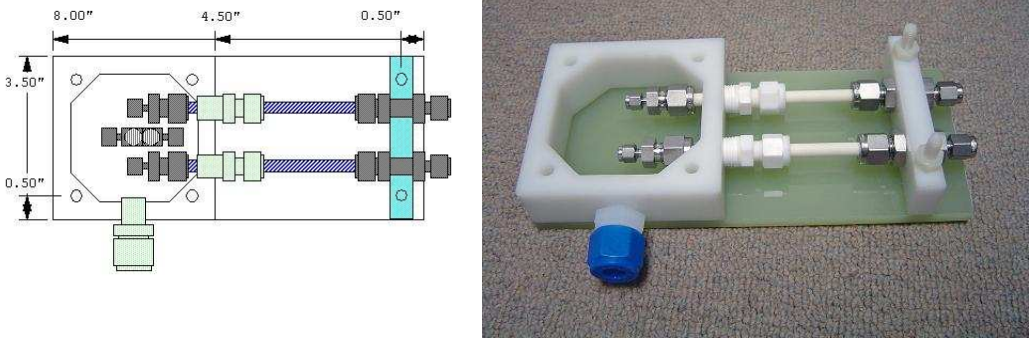

Figure 3-5. Lower grid assembly.

The grid is fabricated out of a continuous length of 1/16" OD stainless tubing. A continuous length of tubing is used to simplify coolant connections, however this required careful planning of the grid construction method. After measuring a length of tubing for the coolant feed, the first grid loop was constructed by bending it around a slotted section of 7/8" OD stainless tubing. (Figure 3-6) After a ring in one direction was formed, the grid was rotated by 90 degrees and inserted into the slot in the tube, allowing the second ring to accurately formed both at the correct angle and alignment to the previous one. After forming 3/4 of the second ring the tubing is bent parallel to the plain the first ring but perpendicular to the coolant feed. The third ring is then formed by inserting the two rings into the slotted pipe section and winding along the axis of

the coolant feed. The last 1/4 of the second ring is then formed and the remaining tubing is used for the coolant return.

Figure 3-6. Grid winding process.

The grid coolant feeds are then insulated by a series of increasing diameter alumina tubes. First a dual bore 1/16" ID, 3/16" OD tube is used to secure the coolant feeds, followed by a 4" long 1/4" OD 3/16" ID tube, then a 6" long (4" long version shown in diagram) 1/2" OD 1/4" ID tube, and finally a 6" long 3/4" OD 1/2" ID tube that is used as the vacuum feedthrough and HV insulator. The surface of the final tube is polished by an 800 grit diamond file while it was spun on a lathe in order to provide a smooth surface for the vacuum seals. (Figure 3-7)

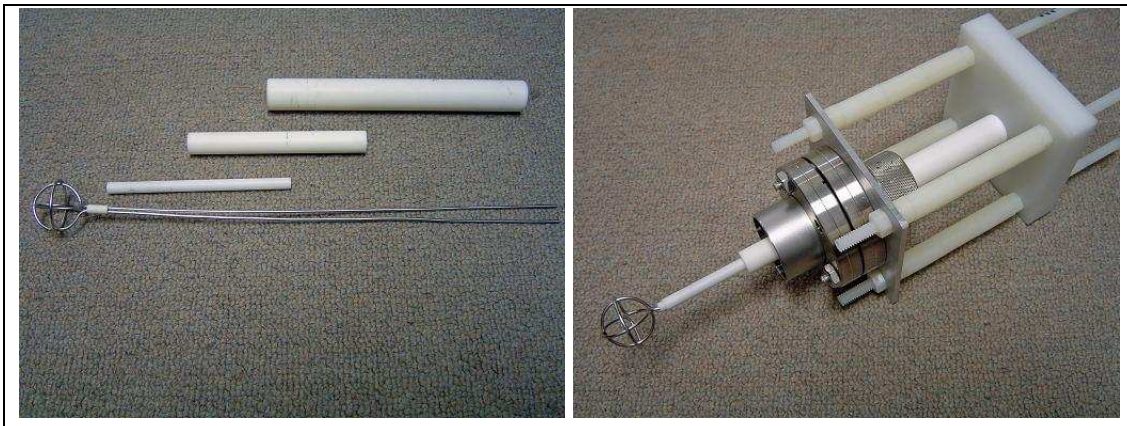

Figure 3-7. Grid insulator assembly.

A vacuum seal for the coolant feeds is established by modifying a 3/4" swagelok tube cap. Two 1/16" holed are drilled 3/8" apart in the face of the fitting allowing the coolant feeds to pas through. A corresponding aluminum plate is fabricated with countersunk holes in a matching pattern and a hexagonal counter bore to align the swagelok fitting. The face of the tube cap is polished allowing a nylon ferule to seal the coolant feeds against the fitting. A teflon ferrule is then used in the fitting to provide a vacuum seal against the alumina tube. (Figure 3-8)

Figure 3-8. Cooling line vacuum seal components.

When the aluminum plate is tightened down, the counter in the holes compresses the ferrules against the coolant tubes, while they are also compressed against the polished face of the tube cap thereby creating a vacuum seal. (Figure 3-9)

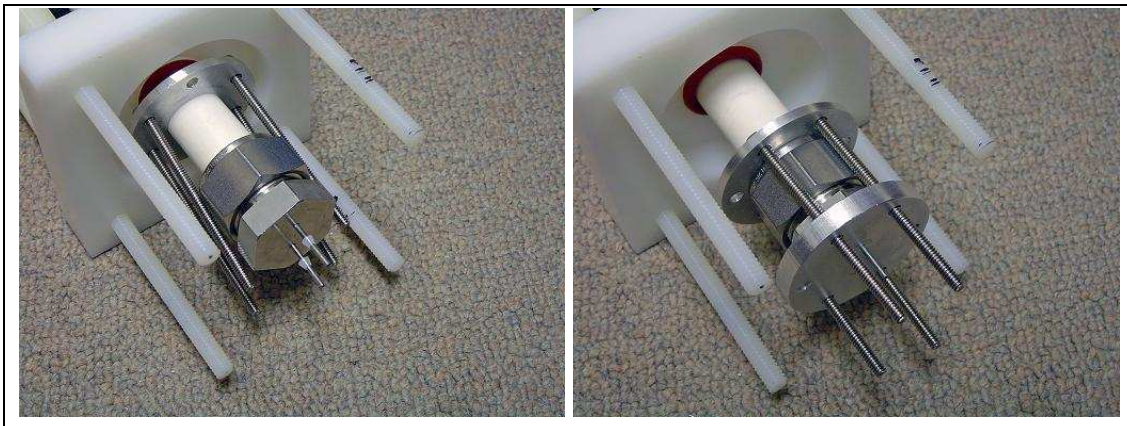

Figure 3-9. Assembly of vacuum seal.

Due to space constraints in the high voltage box, a pair of 1/16" elbows are used to allow the assembly to be more compact. Further this allows the coolant feeds to remain straight. The elbows seal against the coolant feeds with nylon ferules allowing the swagelok nut to be completely removed thereby permitting the ends of the coolant feed to pass back through the holes in the aluminum plate and swagelok fitting allowing the grid to be removed from the assembly during inspection and maintenance. Due to the use of nylon ferrules, an aluminum base plate is used to ensure they do not slip off the coolant lines under pressure. (Figure 3-10)

Figure 3-10. Cooling line adaptors.

The grid system is connected to the ceramic coolant feedthroughs using a 1/16" to 1/4" adaptor with nylon ferrules on the alumina end. The ceramic coolant

feeds are then inserted into the cooling line adaptors and the high voltage box is bolted together completing the grid assembly. (Figure 3-11)

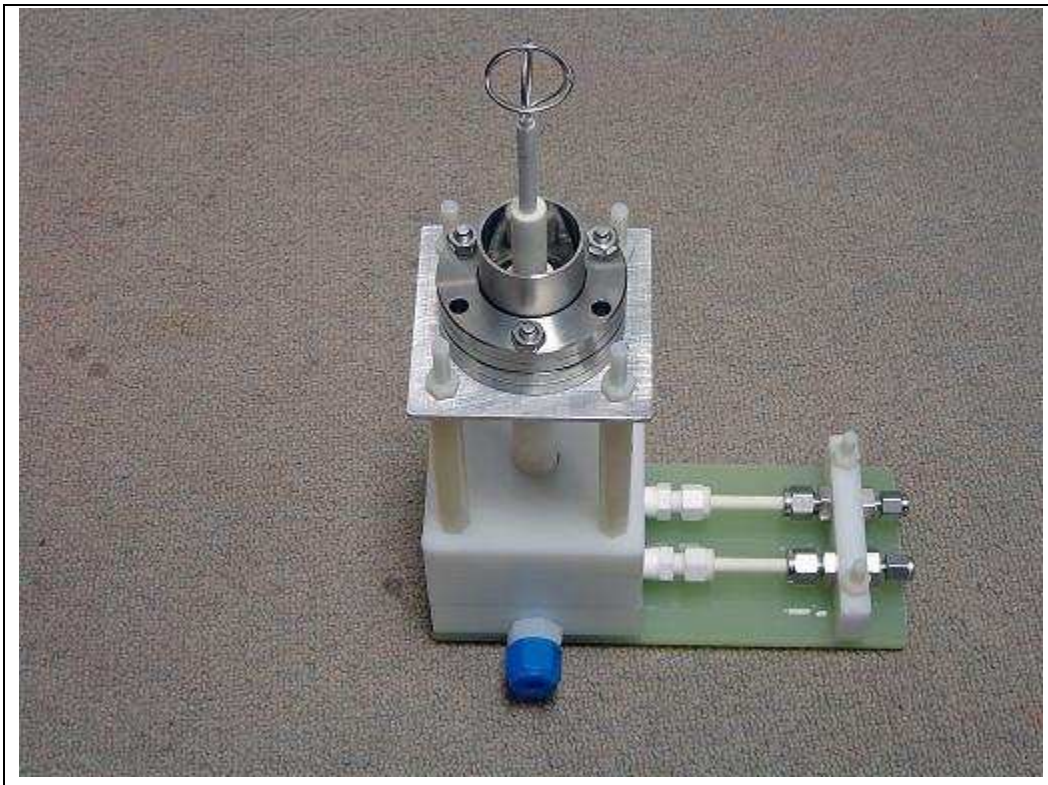

Figure 3-11. Complete grid system.

Grid Cooling System

- **Overview**

The grid cooling system is designed as a dual loop heat exchanger system (Figure 3-12), incorporation both a water and Fluorinert cooling loop. The choice of the dual loop architecture was driven by the requirement of a non conductive coolant flowing across the grid cooling system, and the requirement of a large volume of coolant for use in a radiator system, while using an expensive coolant for the grid cooling loop. The water cooling loop is filled with distilled water and corrosion inhibitors, while the grid cooling loop is filled with Fluorinert FC-40.

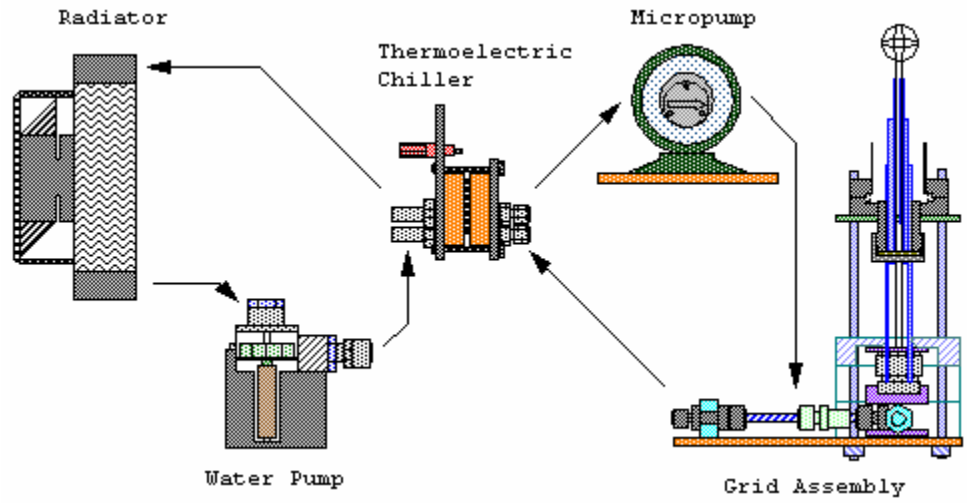

Figure 3-12. Dual loop heat exchanger system.

- **Radiator**

The water cooling loop consists of a computer water cooling system radiator and centripetal water pump. The radiator (Figure 3-13) is mounted on the side of the reactor frame, between the core and the ECRF amplifier. The fan draws air over the reactor core, and force cools the radiator. The exhaust air is routed over the heat sink of the ECRF amplifier, thereby cooling three systems with one fan and saving internal space.

Figure 3-13. Radiator.

- **Water Pump**

The coolant in the water cooling loop is circulated by a Via Aqua 1300 (Figure 3-14) centripetal pump. The water pump mounted with the intake below

the radiator but on the opposite side of the reactor. Positioning the pump intake below the radiator ensures that the pump is always primed when the system is filled with coolant increasing system reliability.

Figure 3-14. Water pump.

- **Heat Exchanger**

The water cooling loop and fluorinert cooling loop are separated by a thermoelectric heat exchanger (Figure 3-15) assembly that increases heat transfer between the cooling loops and allows a smaller volume of fluorinert to be used. The cooled water in the primary cooling loop is pumped through the hot side of a thermoelectric heat exchanger, removing heat from the thermoelectric heat pump used to cool the fluorinert cooling loop. The heat pump consists of two Thermal Enterprises CP1-12710 thermoelectric coolers (TECs) mounted parallel to each other between two copper cooling blocks. Both TECs are coated with Arctic Silver 5 thermal past to increase heat transfer and each is able to pump 85W of heat. The TECs are designed to operate at 12V, however they are electrically connected in series across a 12V power supply; running at 6V. This was chosen to provide a lower heat load on the water cooling loop, thereby providing better performance then if they were each run at 12V. The TECs cool down the cold side cooling block through which the fluorinert is circulated, providing a heat sink for the grid system. The hot side and cold side cooling blocks are compressed together by a pair of aluminum compression plates that are tightened together with 6-32 SS screws. Due to the small screw diameter and

relatively low conductivity of stainless steel, minimal heat is transferred back to the cold side block through the screws.

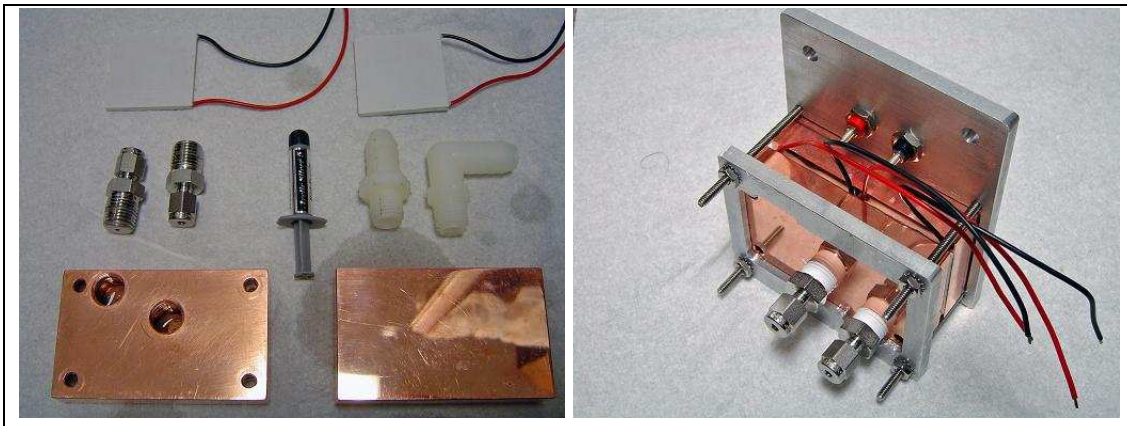

Figure 3-15. Thermoelectric heat exchanger.

Thermocouples are mounted on both the hot side and cold side cooling blocks, allowing heat exchanger temperature to be monitored and providing a method to monitor cooling system performance.

- **Fluorinert Coolant**

3M Fluorinert FC-40 was chosen for use in the grid cooling loop due to its ideal electrical and thermal properties. Fluorinert has several important properties required for the design of the grid system; its low viscosity allows it to be easily pumped through the small bore tubing used to fabricate the grid, its high dielectric value allows it to be pumped across the ceramic break separating the grounded cooling system from the high voltage grid, while its good specific heat allows it to absorb heat deposited on the grid by ion bombardment. (Table 4-1) Additionally, Fluorinert was a high boiling point and is non-flammable, non-toxic, and chemically inert, improving system safety.

However, Fluorinert has the disadvantage of high cost, requiring that the volume used as a coolant is minimized. Further, it has a very low surface contact angle, increasing the probability of leaks, and requiring that the pumping system has no shaft seal.

Table 4-1: Fluorinert Properties

Property	Fluorinert FC-40	Water (distilled)
Boiling Point (℃)	155	100
Density (kg/m3)	1850	998
Kinematic Viscosity (cSt)	1.8	1
Absolute Viscosity (centipoise)	3.4	0.8937
Specific Heat (J /kg-℀)	1100	4184
Dielectric Strength (kV, 0.1” gap)	46	NA
Volume Resistivity (Ω cm)	10^15	2x10^7

- **IDEX Micropump**

The chilled fluorinert coolant from the heat exchanger is circulated through the grid by a GJ series IDEX micropump (Figure 3-16). The micropump is a gear pump and has the advantage of utilizing a magnetic drive, thereby eliminating the potential of leakage of fluorinert around a shaft seal. The pump is capable of a maximum supply pressure of 80 PSI and incorporates an internal pressure relief valve that diverts coolant from the output back to the intake in order to regulate pressure. In operation, bypassing coolant through the pressure relief valve would add heat to the fluorinert coolant loop, and is therefore avoided. The micropump speed is therefore reduced and the system is run at 60 PSI, while the relief valve is set at 80 PSI thereby increasing system performance. At 60 PSI the flow rate through the grid is approximately 0.75ml/s.

A 5 micron Swagelok filter is attached between the micropump and the grid system to remove any particulate matter that in introduced into the system during coolant addition. Due to the narrow gauge tubing used in the grid, the filter was added to prevent particulate matter from clogging the coolant tubes. Additionally, a 100 PSI pressure transducer is attached after the filter to monitor the actual coolant feed pressure to the grid. In this manner, any pressure drop across the filter can be neglected during flow calculations, since the transducer measures actual pressure directly at the grid input.

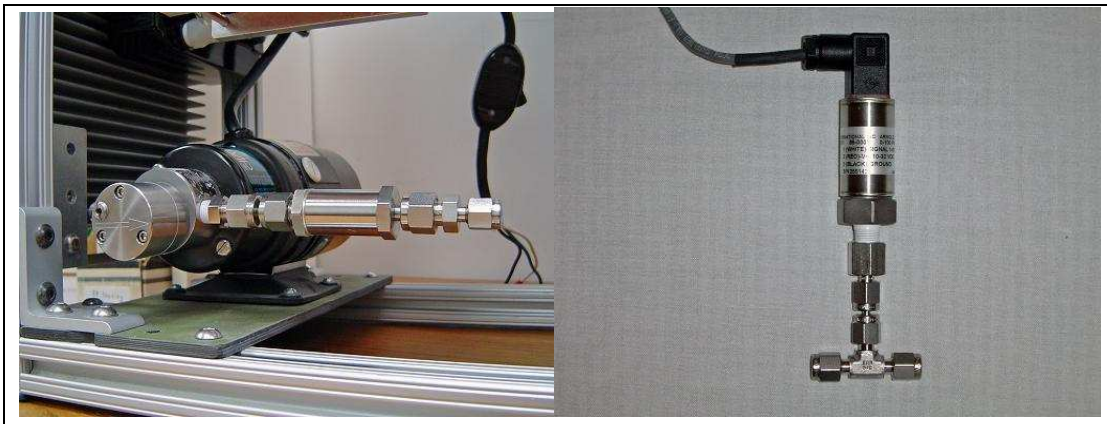

Figure 3-16. IDEX micropump with filter and pressure transducer.

- **Grid Thermocouples**

In order to accurately determine power dissipation into the grid due to ion bombardment, it is necessary to measure the temperature increase in the flowing coolant. A pair of thermocouples have (Figure 3-17) been modified to allow positioning of the thermocouple junction directly within the coolant flow at the entry and exit points of the grid system.

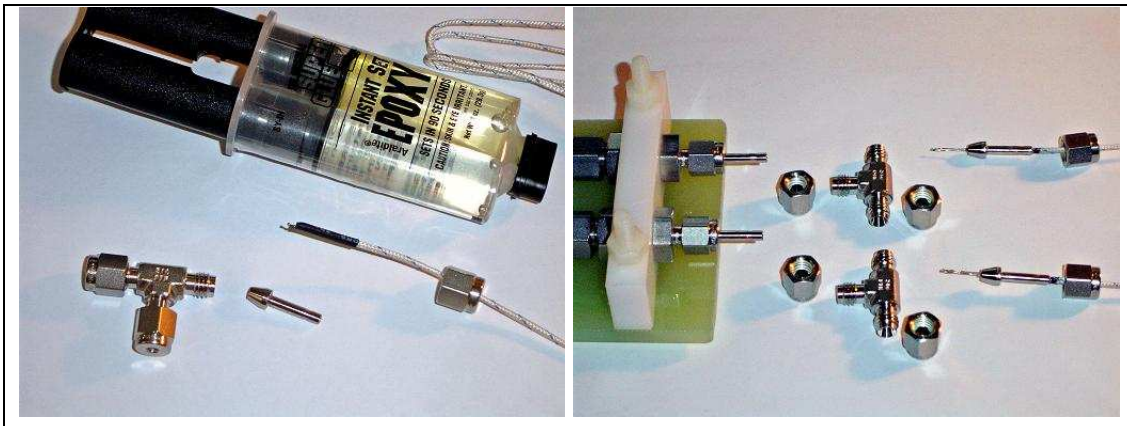

Figure 3-17. Coolant thermocouples.

By positioning the thermocouples directly within the grid coolant feeds, measurement accuracy is improved by reducing the length of exposed metal tubing between the measurement point and the grid system over which convectional losses could occur. Further, by positioning the thermocouple junction within the coolant flow, response time is greatly improved over any

method involving external measurement of the surface temperature of a metal tube.

Deuterium Supply

A deuterium gas handling system is constructed to accurately meter fuel into the reactor and store deuterium produced by a fuel converter unit. The fuel converter unit will allow the reactor to be run off of heavy water, due to the considerably lower cost when compared to high purity deuterium available in lecture bottles. The electrolyte mixture consists of Na_2CO_3 (sodium carbonate) dissolved in heavy water to allow adequate current flow. Sodium carbonate was chosen as the electrolyte due to its high solubility and low corrosive potential

The heavy water electrolyzer contains heavy water in an electrolysis cell consisting of a glass tube with helical platinum coils on the interior and exterior. Oxygen is produced on the exterior coil and is vented into the atmosphere while deuterium is generated on the interior coil and remains trapped within the tube by the water level until it is extracted through the swagelok fitting at the top. (Figure 3-18)

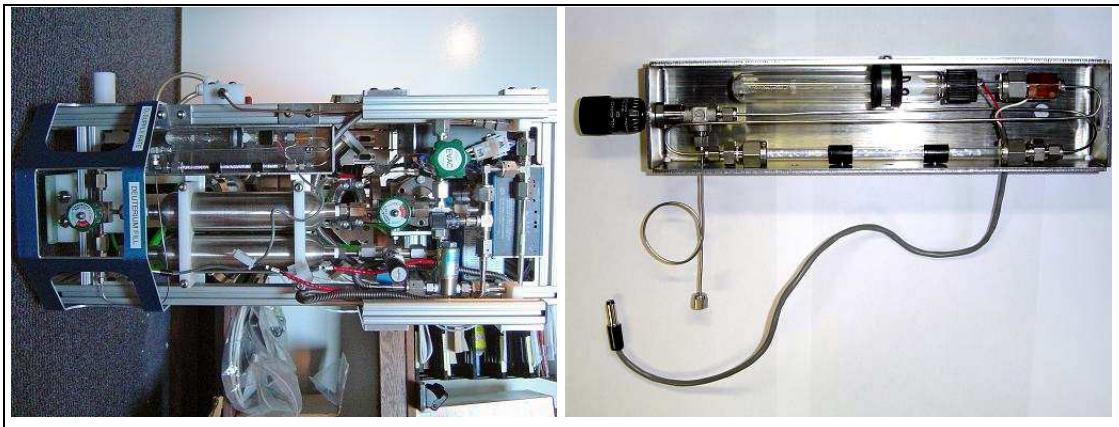

Figure 3-18. Deuterium handling system and heavy water electrolyzer.

The generated deuterium passes through a Drierite column to remove any residual heavy water vapor and is feed into the gas handling system through a

metering valve. The gas handling system consists of a distribution manifold connected to a purge line, a convectron gauge, a set of storage tanks and a mass flow controller for regulating deuterium supply rate into the reactor.

Deuterium is stored in a pair of 300cc swagelok tanks providing 600cc of deuterium storage. The storage tanks are connected to the distribution manifold which allows pressure monitoring and evacuation of the storage tanks. The distribution manifold also connects the storage tanks to a mass flow controller allowing accurate control of the deuterium flow rate between 0 and 10ml/min. Optionally a set of metering valves and solenoids may be used to bypass the mass flow controller allowing higher flow rates or manual control. (Figure 3-19)

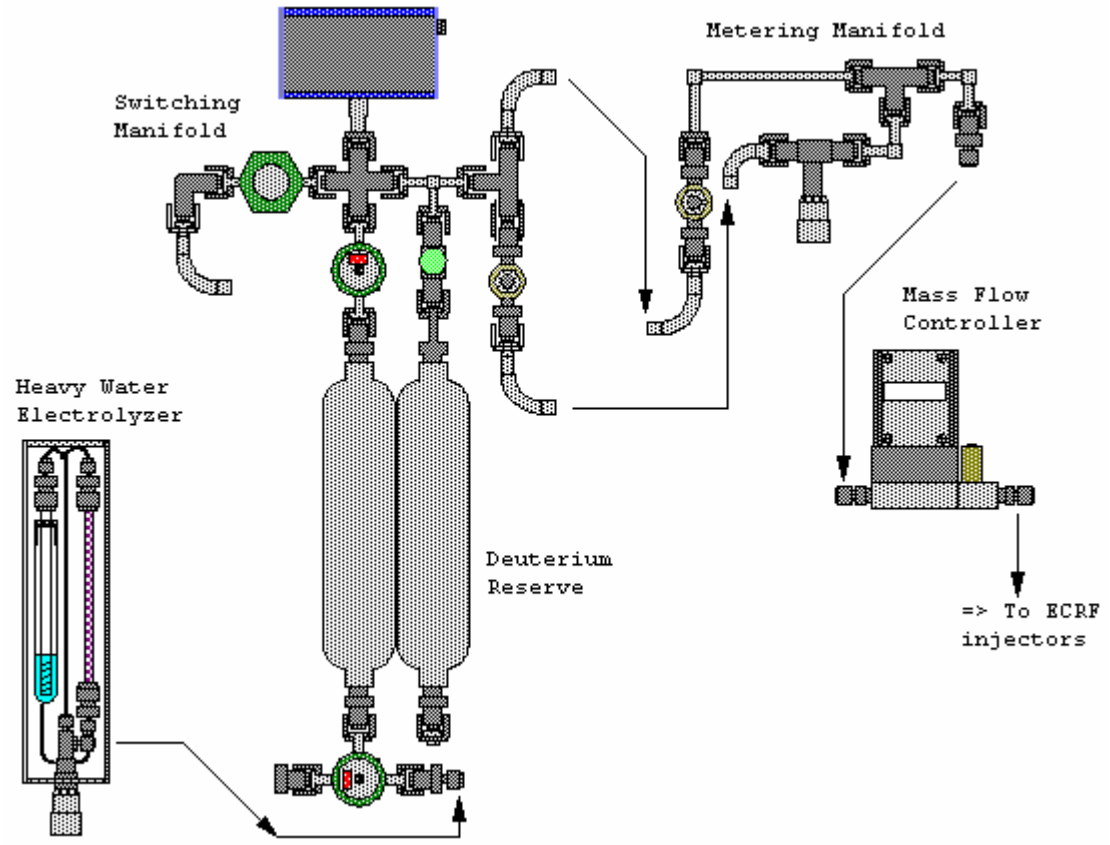

Figure 3-19. Deuterium handling system.

Reactor Vacuum Chamber

The reactor core consists of a 304 SS spherical vacuum chamber equipped with 8 off axis ports for ion injectors and instrumentation, and two on axis ports for vacuum system connection and grid feedthroughs. The spherical vacuum chamber is constructed out of a pair of 6" diameter, 1/8" thick hemispheres coupled together with 8” rotatable conflat flanges. Each off axis port consists of a 2.5" long 2.75” conflat half nipple equally positioned 90 degrees apart in azimuth and 45 degrees in elevation off the vertical axis. The on axis ports consist of 1.5" long rotatable 2.75” conflat half nipples. (Figure 3-20) Each of the ports is aligned so that the relative axis of each port intersects at the center of the hemisphere, allowing deuterium beams from each of the ion injectors to converge at a focal point in the center of the accelerating grid.

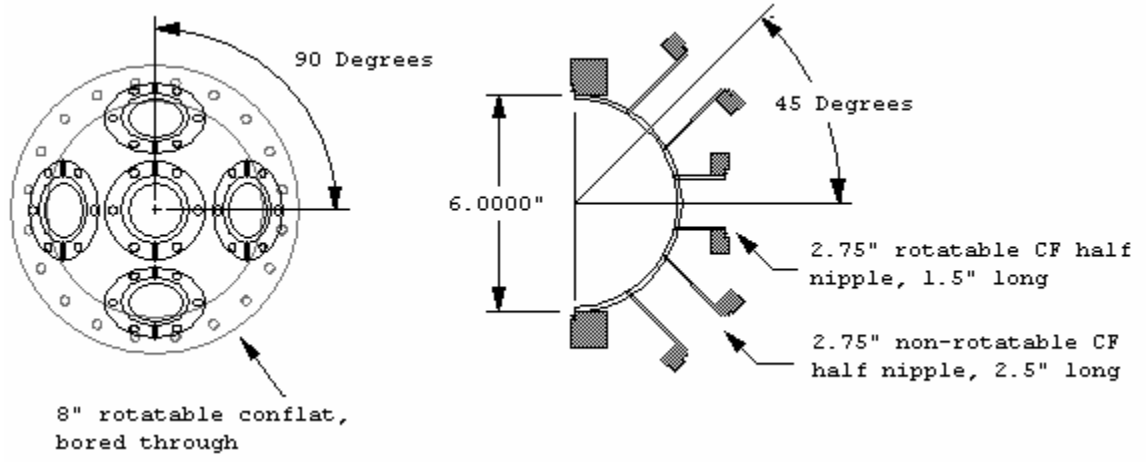

Figure 3-20. Hemisphere dimensions.

The holes bored in the hemisphere to accommodate the conflat nipples are 1.495” in diameter to ensure a snug fit of the half nipple, thereby ensuring a good quality TIG weld. The 8” rotatable conflat flanges are turned down on a lathe, removing the internal weld lip and allowing the face of the hemisphere to be positioned flush to the face of the rotatable conflat ring. To compensate for the thickness of the o-ring used to seal the 8” conflat flanges together, 0.045” is

removed from the height of the hemisphere, thereby ensuring the vacuum chamber remains spherical when assembled.

The interior and exterior of the hemispheres are polished with up to 2500 grit silicon carbide sandpaper. The smooth interior surface will enable the reactor to be cleaned more effectively as fewer contaminants would be trapped in the surface. The core was not electro-polished as this would form a passivation layer that would interfere with the TIG welding process.

To allow electrical insulation between the hemisphere halves, a viton o-ring was chosen as the vacuum seal. The electrical insulation will allow monitoring of the fraction of the current deposited into each hemisphere during future experimentation, as well as the possibility to bias each hemisphere at a different potential.

In preliminary experimentation it was observed that plasma bombardment of the o-ring would etch the o-ring and cause a large amount of out gassing making it impossible to achieve suitable vacuum levels. To solve this problem an alumina fabric plasma limiter was installed to prevent plasma bombardment of the o-ring thereby solving the out gassing problem.

The plasma limiter consists of an extreme temperature alumina wire loom of 1/4" outer diameter that is compressed between the faces of the hemispheres thereby shielding the o-ring from plasma bombardment. (Figure 3-21) To prevent out gassing of the limiter, the alumina loom was baked out at approximately 2500℃ for one hour to remove binding agents introd uced during the manufacturing process.

Figure 3-21. Welded hemisphere and alumina fabric plasma limiter.

Vacuum System

The reactor core is connected to a high performance vacuum system to reduce the system pressure to 1 mTorr in order to reduce ion-neutral collisions in the reactor and prevent Paschen breakdown between the accelerating grid and the grounded reactor shell. The reactor core contains a vacuum hub connected to the top hemisphere of the vacuum chamber. The vacuum hub connects to the reactor core, vacuum sensors, purge lines from the deuterium handling system and to the external vacuum pumps through a computer controlled throttling valve.

The throttling valve is controlled through a PID control loop implemented in Labview deriving its feedback from a series of convectron vacuum gauges. In this manner the reactor can accurately maintain a stable core pressure over a wide range of operating conditions and fuel supply rates.

The exhaust line of the vacuum hub will connect to an external vacuum system consisting of a 300 l/s turbomolecular pump backed by a dual stage direct drive vacuum pump. (Figure 3-22) The addition of the turbo pump will allow operating the reactor into pressures below 1mTorr, and at high fuel supply rates, where the backing pump alone would not be capable of maintaining the required pumping performance.

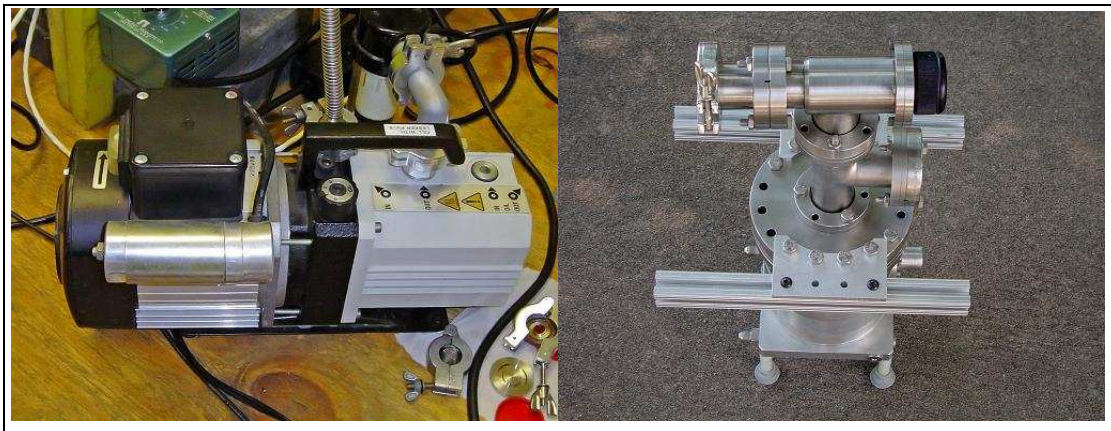

Figure 3-22. Backing pump and turbo pump.

Power Supply

The central grid is connected to a high voltage power supply capable of sourcing -50 kV at 30 mA to accelerate ions. An x-ray transformer was chosen due to its low impedance and capability to source current in the 100s of mA if run at very low duty cycle. The transformer chosen for this experiment is rated at 100kV differential voltage 30mA current (Figure 3-23).

Figure 3-23. X-ray transformer and mount.

The secondary winding of the transformer is center tapped, allowing only half of maximum differential voltage to be generated with respect to ground. The AC output of the transformer is then full wave rectified by an x-ray rectifier. The rectifier consists of a pair of 150kV rated diode assemblies in parallel connected to the output of each secondary coil. The diode assemblies for each coil are connected to the high voltage output terminal mounted on the transformer tank while the primary coil is connected to the 120VAC mains through a set of 1/4-20 bolts that pass through the top of the bucket. (Figure 3-24)

Figure 3-24. AC and high voltage connectors.

Both the transformer and the rectifier assembly are mounted onto a high density polyethylene holder which is positioned within a 3 gallon bucket that acts as the transformer tank. The tank is filled with mineral oil for cooling as well as electrical insulation of the rectifiers and transformer. (Figure 3-25)

Figure 3-25. Oil tank and control electronics.

Current sourced by the transformer is monitored by placing a 100 ohm resistor between the secondary center tap and ground, thereby providing a voltage signal of 0.1V/mA. The high voltage output is monitored with a fluke 10K-40 high voltage probe providing a 1000:1 ratio voltage divider. (Figure 3-26)

Power output from the transformer is controlled with a solid state phase angel controller (PAC). The PAC provides power control proportional to a 1-5V input signal from the control computer, and triggers a random fire solid state relay to connect the transformer to the AC input at a varying position on the AC cycle.

During data collection, the PAC was bypasses and a variac was used to control power for safety and stability reasons.

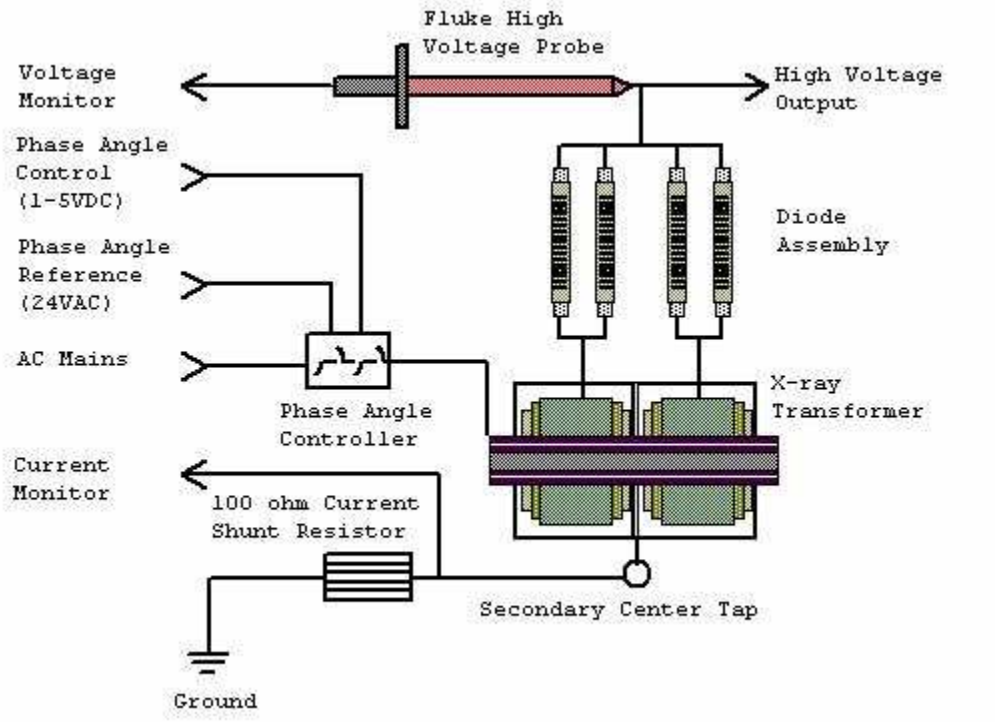

Figure 3-26. X-ray transformer electrical diagram.

Control System and Electrical Power

The control system consists of a combination of manual and computer based monitoring and control elements. The top control panel of the reactor contains a 3 position rotary power switch, scram button and interlock switches for the high voltage supplies powering the ion injectors and grid assembly as well as selector switches for the fuel control system. (Figure 3-27)

The power selector switch can be set to either standby or run mode. In standby, only the control systems are powered while in run mode the cooling system is powered as well and the high voltage supplies are enabled. The scram switch shuts down the high voltage supplies, the fluorinert pump, and the thermoelectric heat exchanger.

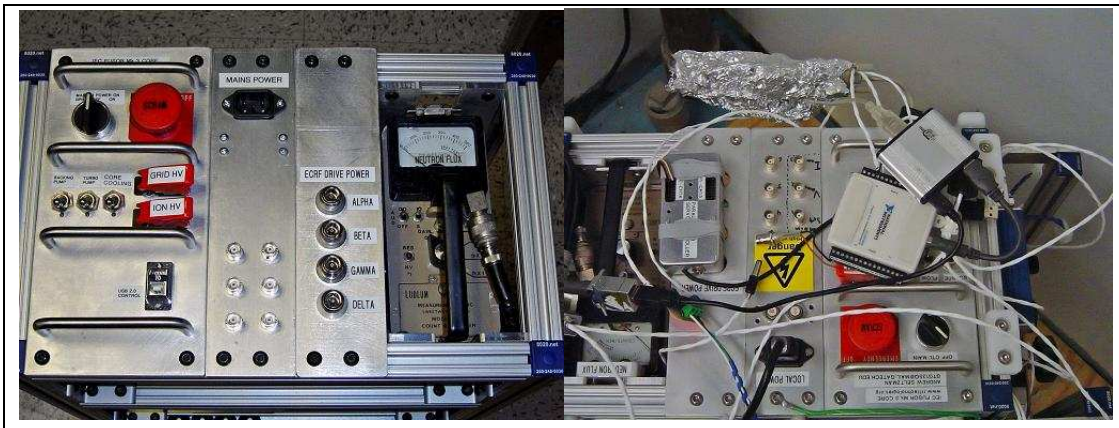

Figure 3-27. Control panel and computer control system.

The computer control system was designed to connect to the control laptop through a single USB port in order to simplify operation. The reactor is controlled in Labview allowing real time system monitoring and data logging. The USB connection to the reactor system is distributed by a 4 port USB hub to a servo controller, a thermocouple interface and a National Instruments USB-6008 data logger. The servo controller is manufactured by Parallax inc and provides 16 PWM servo channels for use with hobby servos such as the one used to control the vacuum system throttling valve. Additionally the servo controller has a built in USB to serial converter based off of the FTDI chipset allowing simple integration with the USB control bus. (Figure 3-28)

Thermocouples monitoring cooling system temperatures are interfaced with a set of 4 Analog Devices AD6B11 thermocouple modules that interface with the USB control system through an external USB to serial converter.

Analog and digital I/O is handled by the NI USB-6008 interface allowing monitoring of reactor vacuum levels through the convectron gauge and cooling system pressure through the pressure transducer as well other non-critical required I/O functions.

Figure 3-28. Thermocouple interface and servo controller.

ECRF Ion Injector

There are four injectors mounted within the 3" long conflat half nipples. Each injector is expected to produce a 10 mA beam of deuterium at 15 KeV energy. The RF drive system will consist of a Mini-circuits VCO and mixer for frequency and amplitude control connected to an intermediate pre-amplifier driving a high power booster amplifier capable of 200 W output. The amplifier will have dual input/output channels, each of which will drive an ion injector pair through a power splitter. The ECRF injector drive coil is designed numerically in NEC2, and optimized for impedance matching and field geometry to provide maximum excitation of the ECRF resonance in the plasma while reducing reflected power from the injector system. The injectors extractor potential is provided by a Hitek 3000 power supply which will bias each drive coil at +15 kV, repelling the deuterium ions through the grounded extractor cone. If deemed necessary, an einzel lens will then be used to further focus the deuterium beam, thereby providing a sharper focus and increasing plasma density. (Figure 3-29)

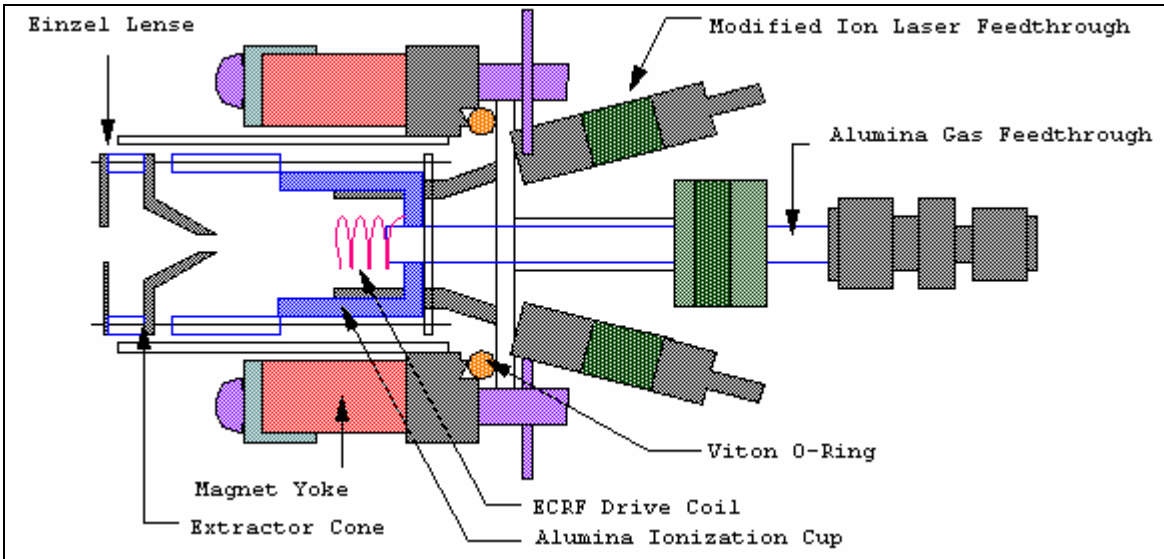

Figure 3-29. ECRF ion injector.

Recommended Modifications to Current Design

Certain elements of the reactor design were constructed in a non ideal manner due to the use of parts on hand or the adaptation of currently used components from previous designs that did not meet required operation standards. Many of these issues could have been resolved with minimal modification, however, they were not modified due to their sufficient operation and the need to start collecting data. A list of known problems and proposed solutions have therefore been compiled such that

- **RF coupling between grid feed through and thermocouple interface module.**
    - The thermocouple lines run vertically along the reactor frame, near the grid feedthrough. During operation RF noise is coupled into the thermocouple system if sudden discharges occur. While the thermocouple system is partially immune to interference, the RF can couple through the thermocouple reader into USB interface

components, causing them to disconnect from the control computer.

- **RF interference with USB to serial convertors.**
    - RF interference can couple into the USB to serial converters used in the control causing them to disconnect. RF filtering on the serial lines or industrial grade converters may solve this problem.
- **Ferrule orientation on grid vacuum seals.**
    - As designed, the tips of the Swagelok ferrules insert into a conical bore in the aluminum compression plate while the rear of the ferrule is compressed against the polished surface of the Swagelok fitting creating a vacuum seal. Ideally, the tip if the ferrule should insert into a conical bore in the Swagelok fitting, thereby creating maximum compression at both vacuum sealing interfaces.
- **Non-parallel connections of swagelok tanks.**
    - The separate 300mL deuterium storage tanks and not connected in parallel due to problems aligning several VCR components. One tank is connected in series with the deuterium source, while the other is connected parallel to the distribution manifold. Ideally both of these tanks should be in parallel with the manifold.
- **Servo valve linkage.**
    - The throttling valve is currently connected to the control servo through a linking rod, however this setup does not provide enough force at the end positions to unseat the valve when it is closed. This can be improved by directly driving the valve through a gear assembly instead of the linking rod.
- **Heavy water electrolyzer thermal management.**
    - The electrolysis of the heavy water generates a small amount of heat that eventually heats up the reservoir. The increased temperature increases the amount of heavy water vapor mixed in with the deuterium gas, shortening the life of the Drierite column.

This problem could be eliminated by mounting the base of the electrolyzer in a heat sink.

- **Electrolyser heavy water level monitoring.**
    - There is no method of limiting the flow of deuterium to prevent the heavy water from being drawn up into the Drierite column. It is possible to set a high enough deuterium flow rate for this to occur. It would be advantageous to install an automatic heavy water level monitoring system to reduce deuterium flow when the level in the central tube starts to rise.
- **Vacuum system valving.**
    - Additional valves on the reactor system to isolate the turbo pump from the backing pump, vent the reactor to atmosphere, and connect the system to an external deuterium source would increase the ease of operation.

Detailed Design Documentation

Detailed documentation of reactor construction including dimensioned cad files, CNC mill code, and step by step construction procedures are beyond the scientific scope of this document and as such are not included. Complete documentation may be obtained by contacting the author or visiting www.rtftechnologies.org where complete documentation has been posted.

CHAPTER 4
RESULTS

Results Overview

Reactor data was acquired in the glow discharge and high pressure star discharge regions between pressures of 31mTorr and 13mTorr (Figure 4-1). Due to the lack of an operational ECRF ion injector at the time of data acquisition, the reactor could not maintain a stable plasma discharge below 13mTorr. Below this pressure, the plasma discharge would extinguish and could not be initiated by increasing the voltage applied to the grid up to -20kV. An ion source consisting of a 100W light bulb filament driven at 12V was used to assist in providing a stable source of ions towards the lower pressures acquired.

For safety reasons, the grid voltage was limited to -20kV by the use of resistive ballast in series with the primary winding of the x-ray transformer used to power the grid. The resistive ballast was chosen to limit current draw should the insulator system arc over, thereby minimizing any thermal damage that might occur to reactor components. The resistive ballast was only used for testing above -15kV where it was not known if the grid insulators would arc over. For operation below 13kV no ballasting was used, thereby allowing higher current operation.

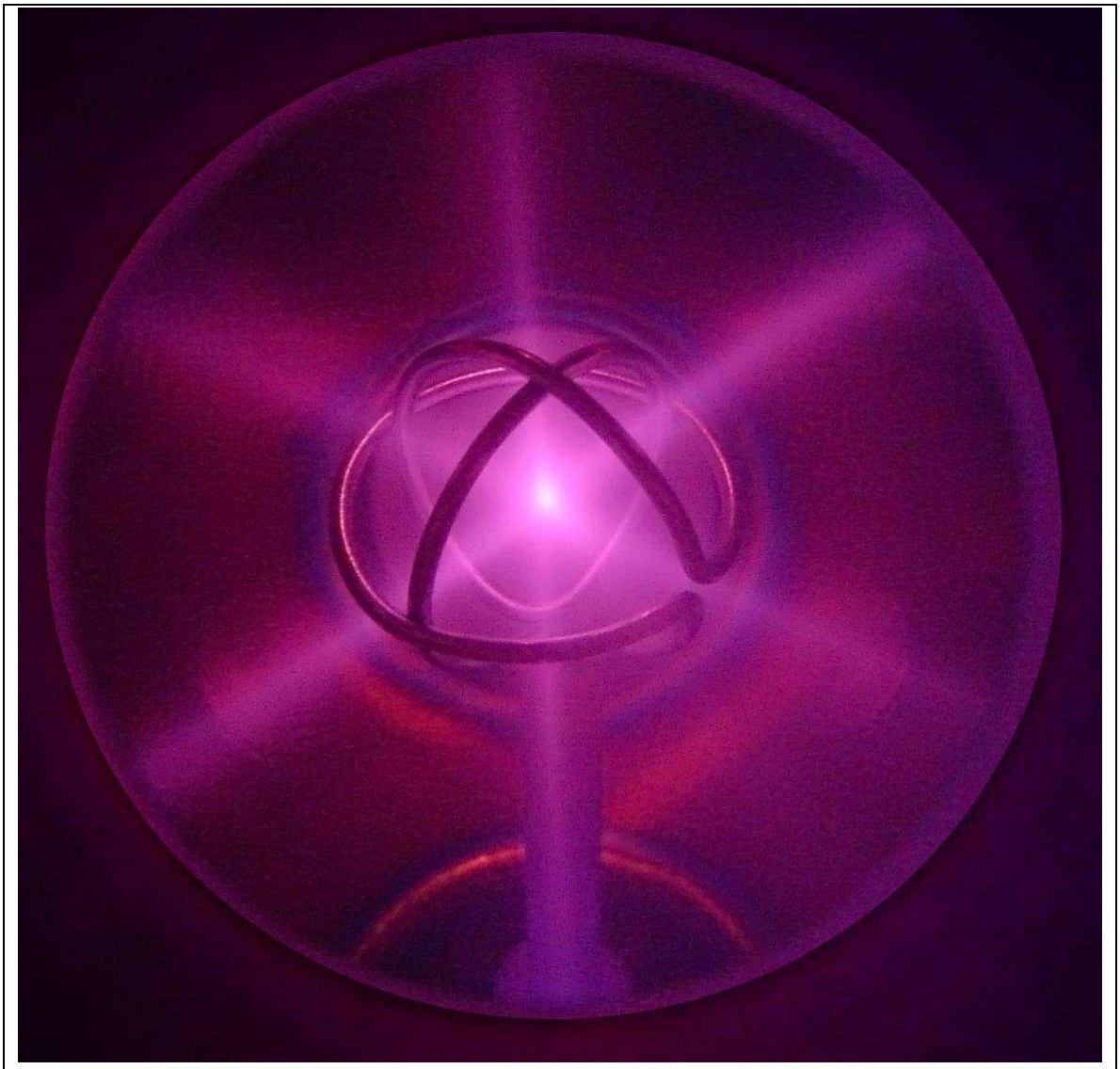

Figure 4-1. Plasma focus at 13kV, 5mA, and 16mTorr.

Grid Cooling Data Acquisition

The use of an actively cooled grid allows direct measurement of grid heating as a function of heat removed by the cooling system. The cooled grid system incorporated both temperature and flow measurement instrumentation to allow accurate quantification of grid heating. The cooled grid system is constructed with thermocouples immersed in the cooling flow immediately before the ceramic electrical breaks on the grid, increasing measurement accuracy by allowing the coolant temperature to be determined before significant conductive

or convective cooling occurs while flowing through the feed and return tubes. A pressure transducer measures coolant feed pressure at the input to the grid system allowing flow rate to be determined. It was assumed that the flow rate was proportional to pressure.

Reactor pressure was measured by a convectron gauge located at the outer vacuum port of the vacuum hub, before the throttling valve. To enable accurate pressure measurements, the throttling valve was fixed at its full open position, and the vacuum pumping rate was controlled with the vacuum valve at the turbo pump intake. This allows the pressure in the vacuum hub to remain the same as the interior of the reactor by reducing flow rate through components that might incur a pressure drop.

During preliminary testing, the grid coolant (Fluorinert FC-40) flow rate was measured to be 1ml/s at 80 PSI feed pressure by use of a known volume, pressure transducer and timer. The micropump was run at its maximum rated pressure of 80 PSI as measured by the pressure transducer, and the time required to fill a 10ml syringe casing was measured to be 10 sec. The micropump in use included an overpressure bypass valve that was set to open near 80PSI, diverting pressurized coolant back to the pump intake to relieve overpressure. Due to viscous and frictional losses as well as pump slip, it was found that operating the pump near 80 PSI caused increased coolant heating within the pump system, thereby decreasing cooling system performance. During reactor operation, the cooling system pressure was reduced to 60 PSI (approximately 0.75ml/s), thereby reducing the fraction of the coolant diverted through the bypass valve and increasing cooling system efficiency. It was found that the reduced coolant flow did not significantly increase the maximum grid temperature, as indicated by coolant temperatures remaining below 45℃ at the maximum electrical drive power of 155W. Since the grid temperature remained near that of the reactor shell, it can be approximated that radiative heat transfer away from the grid is negligible compared to heat removed by the cooling system and therefore can be neglected in grid heat load calculations. Cooling system

data was automatically logged in Labview, and temperature readings were acquired after coolant input and output measurements had stabilized to compensate for any time lag generated by the thermal mass of the grid system.

At the time of these tests, neither the solid state phase angle control for the x-ray transformer, not the NI interface to automatically log grid voltage or current through Labview were operational. The x-ray transformer was controlled manually through a variac, while grid voltage and current were logged manually with digital multimeters. A Fluke 80k-40 40kV high voltage probe was used to measure grid voltage, while grid current was measured by the voltage drop across a 100 ohm resistor in series with the grounded center tap of the x-ray transformers secondary winding. Both voltage and current readings were stable with only minor fluctuations on the readouts.

Grid Cooling Data

The grid coolant loop containing Fluorinert FC-40 was run at 60 PSI equating to a flow rate of 0.75 ml/s. Using the thermocouples located on the coolant feed and return ports of the grid assembly, the temperature increase of the coolant was measured and used to calculate the power load dissipated into the grid (denoted “H: Grid Heating (W)”) by ion bombardment heating. Grid voltage (denoted “Drive Voltage (kV)) and grid current (denoted “Drive Current (mA)) were measured directly with monitoring instrumentation on the transformer assembly. Electrical input power to the grid assembly (denoted “P: Drive Power (W)”) was determined by the product of average voltage and current sourced by the x-ray transformer. DC impedance of the grid in Mohms (denoted “Z(Mohm)”) was calculated by dividing drive voltage by drive current. Grid heating power fraction H/P was calculated as Grid Heating divided by Drive Power and represents the fraction of electrical input power that is dissipated into heating the grid.

Grid Temperature vs. Drive Power

Maximum Grid Temperature was plotted as a function of Drive Power (Figure 4-2). It was to be linear with drive power at all pressures.

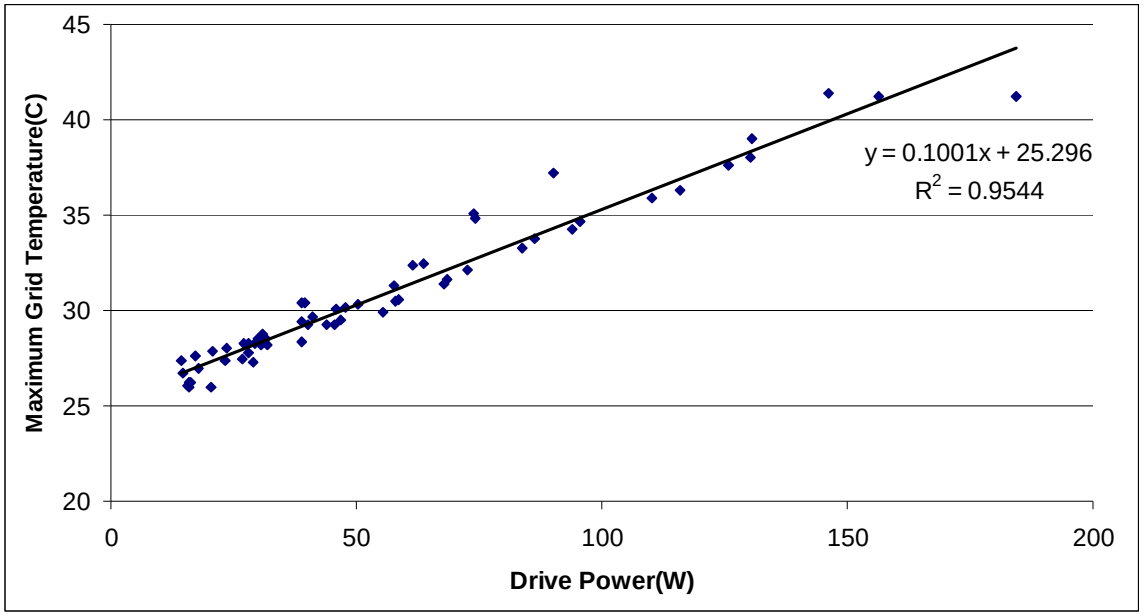

Figure 4-2. Maximum Grid Temperature (C) as a function of Drive Power (W).

Grid Heating vs. Drive Power

Grid Heating was plotted as a function of Drive Power (Figure 4-3) at varying pressures. It was observed that the slope decreased with decreasing pressure indicating that as reactor pressure decreases, a smaller fraction of the electrical input power is dissipated into the grid.

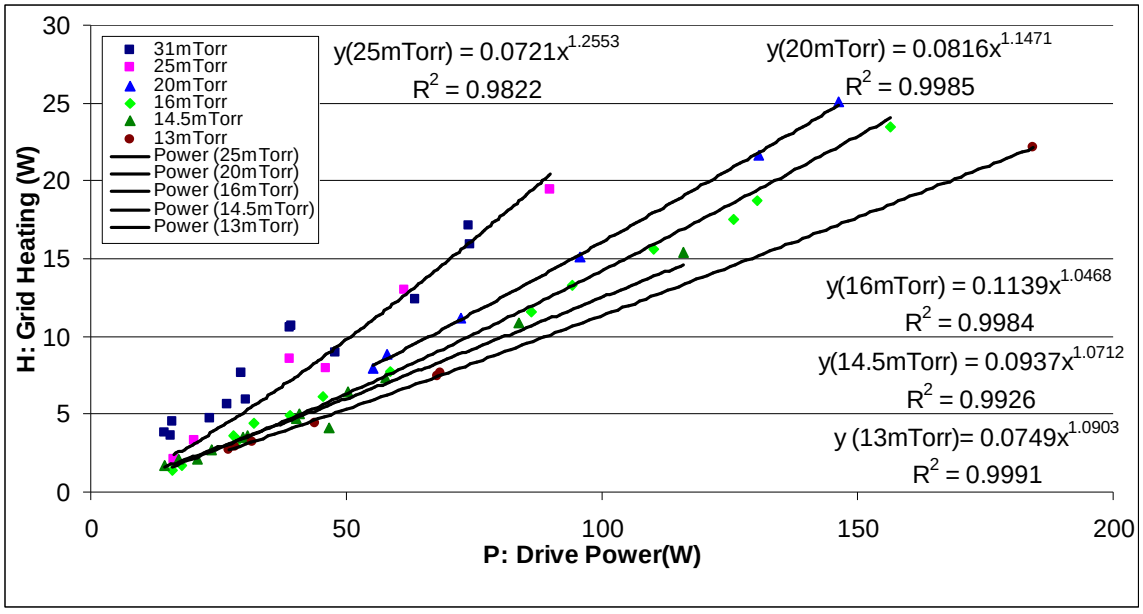

Figure 4-3. Grid Heating (H) as a function of pressure and Drive Power (W).

Grid Impedance vs. Drive Power

Grid impedance was plotted as a function of Drive Power (Figure 4-4) at varying pressures. It was observed that at high pressures plasma impedance was independent of drive power, while at lower pressures impedance was related to drive power through a power fit. As pressure decreased it was observed that the negative exponent in the power fit increased in magnitude, indicating that decreasing pressure caused the plasma impedance to vary non-linearly with respect to pressure to a greater extent.

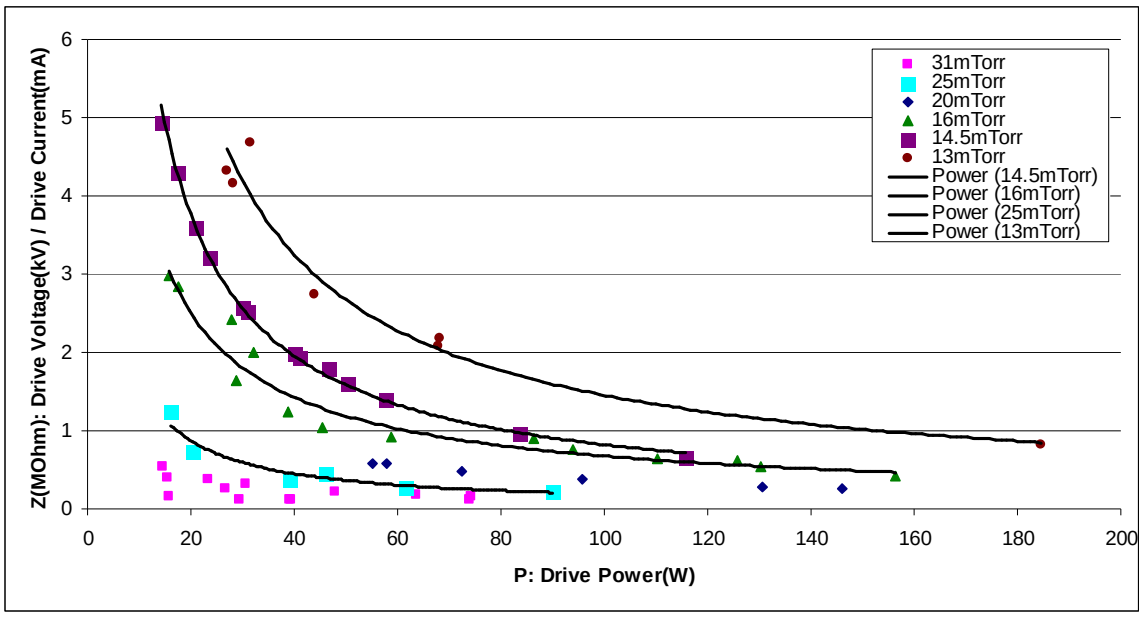

Figure 4-4. Grid impedance (Z) as a function of pressure and Drive Power (W).

Grid Heating Fraction vs. Grid Impedance

Grid Heating Fraction was plotted as a function of grid impedance (Figure 4-5) at varying pressures. The value of Z may be determined from the plot of Z vs. P (Figure 4-3). As Z increased, H/P asymptotically decreased towards a value of 0.1 indicating that the fundamental limit of grid transparency would prevent any less then approximately 10% of the drive power input from heating the grid.

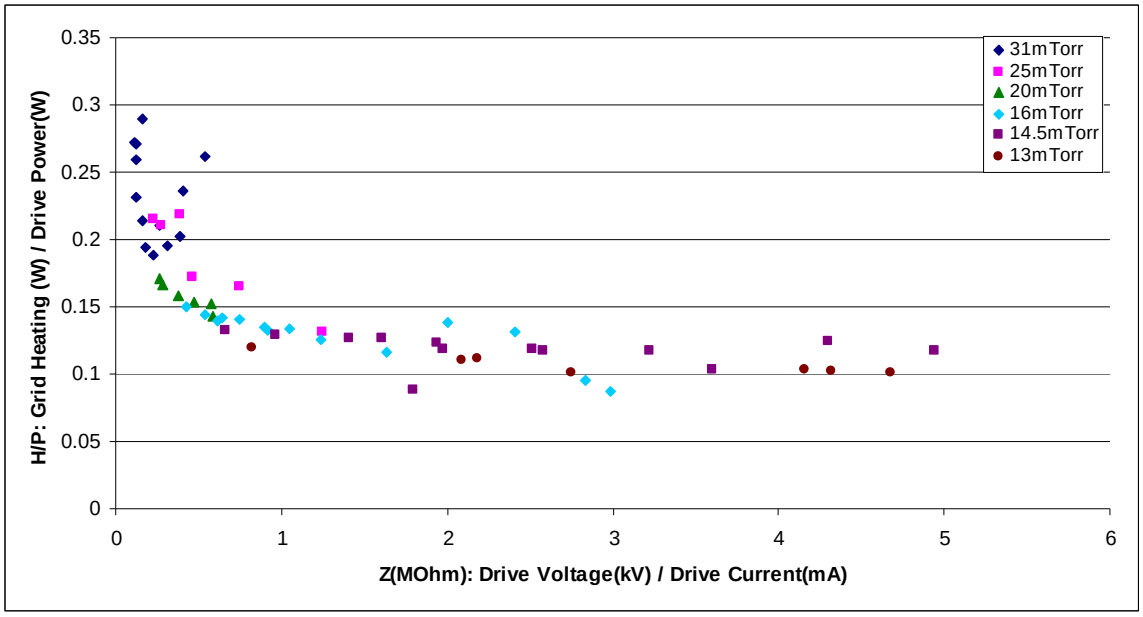

Figure 4-5. Grid heating fraction (H/P) as a function of pressure and grid impedance (Z).

Secondary Electron Emission vs. Ion Energy

Secondary Electron Emission was plotted as a function of Ion Energy (Figure 4-6) at various pressured. Secondary emission rates show and increasing trend with relation to ion energy.

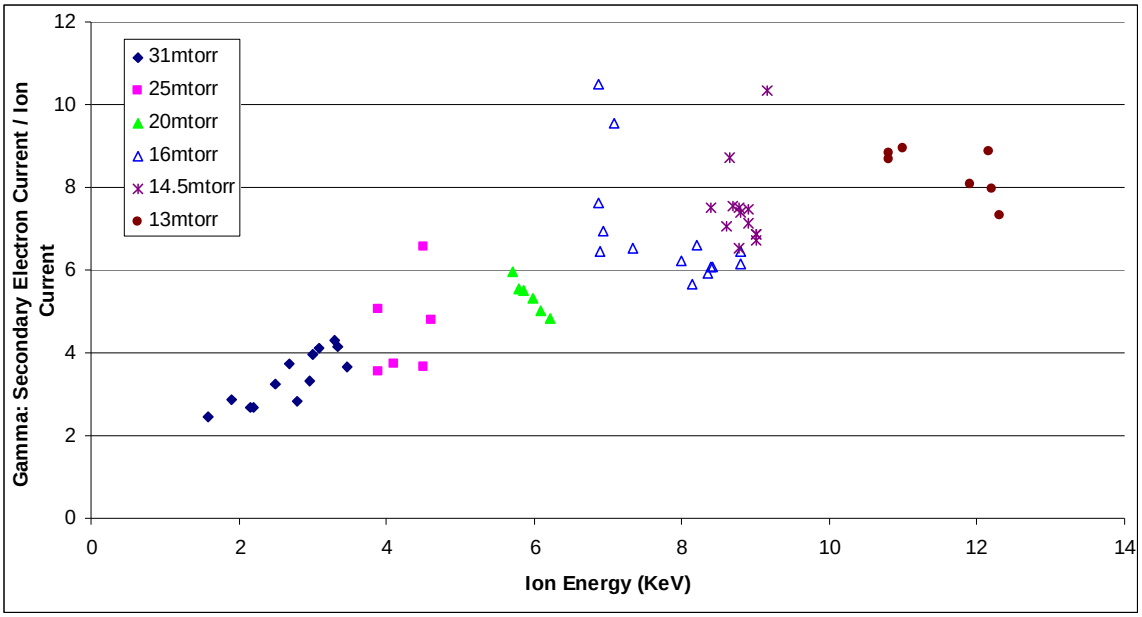

Figure 4-6. Secondary Electron Emission as a function of Ion Energy.

Grid Heating Fraction vs. Secondary Electron Emission

Grid Heating Fraction was plotted as a function of Secondary Electron Emission (Figure 4-7) and found to be strongly correlated for all pressures. As secondary emission rates increase, grid heating fraction decreases.

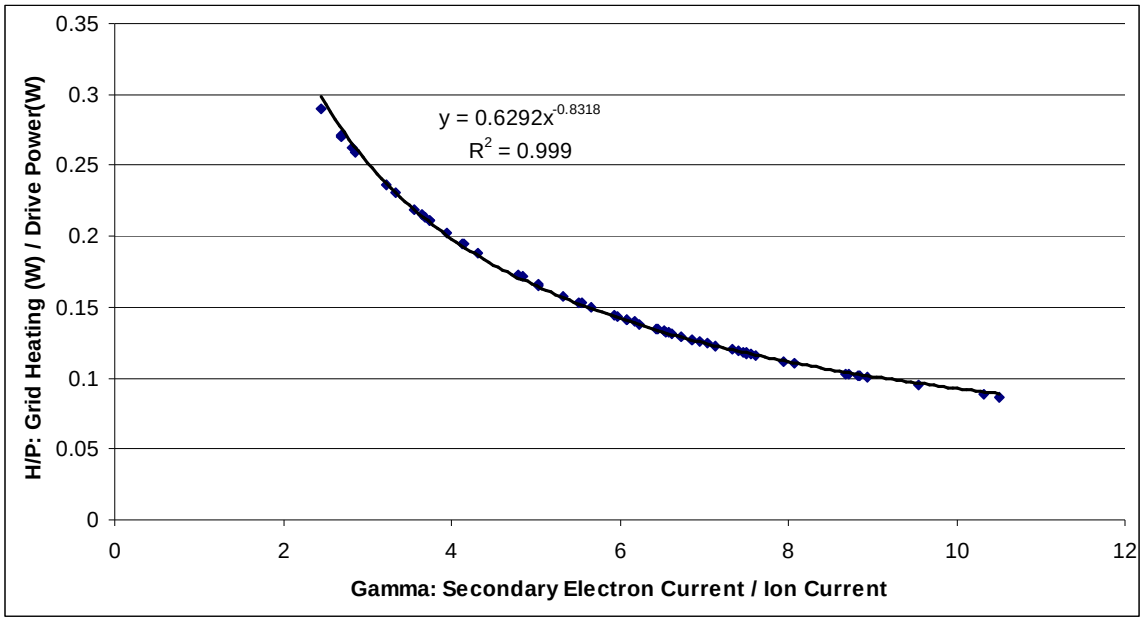

Figure 4-7. Grid heating fraction (H/P) as a function of Secondary Electron Emission

CHAPTER 5
DISCUSSION

Cooling System Operation

The cooling system was found to provide adequate cooling, maintaining a low grid temperature and thereby suppressing thermionic electron emission. A linear fit of the grid temperature to power input graph predicts that grid temperature is essentially linear with respect to drive power. The best fit function of T(C)=0.1(DP) + 25.3 indicates a 0.1℃ increase i n grid temperature above ambient temperature per watt of drive power. Based on the 155℃ boiling point of the Fluorinert FC-40 coolant, it is predicted that the grid assembly will be able to handle up to 1.3kW of drive power allowing for operation at increased plasma density, thereby increasing fusion rates. This power level could be further increased by increasing coolant flow rate, increasing cooling capacity of the thermoelectric heat exchanger, or switching to a Fluorinert type with a higher boiling point.

Reactor Analysis Based on Grid Heating Measurement

The results provided by analyzing the grid heating data may be used to characterize the fundamental physics and operating regions of IEC fusion devises.

It was observed that as reactor pressure decreased, the slope of the H vs. P curve (Figure 4-3) decreased, indicating that the reactor is operating more efficiently at lower pressures. As pressure decreases, a smaller fraction of the input power is dissipated into the grid allowing for higher power operation and increased grid voltage.

The curves plotted for Grid Impedance vs. Drive Power (Figure 4-4) may be accurately fitted as power functions at each given pressure. It was observed that as pressure decreased, the dependence on the exponent increases leading to a more rapid increase in impedance as input power decreased. This may be attributed to lower levels of ionization within the reactor as the plasma discharge

approaches extinction, and therefore fewer ions bombarding the grid, thereby generating a current flow by neutralization and secondary electron generation. At higher power levels, the greater number of circulation ions generates a greater current draw, thereby decreasing impedance. At higher pressures the impedance is nearly constant, corresponding to regions of glow discharge, where a current flows through a diffuse plasma to the reactor walls in contrast to low pressure operation where there exists a distribution of oscillation ions in the volume of the reactor and a dense plasma only at the focal point.

The curves plotted for Grid Heating Fraction (H/P) vs. Impedance (V/I) (Figure 4-5) indicated a decreasing trend in H/P as Z increased. It was observed that H/P was independent of pressure, varying only with respect to Z. The transition region between a diffuse glow discharge in the plasma and discrete oscillation ions may be easily observed in this plot and occurs at approximately 1Mohm and is only attainable for plasma pressures above 14.5 mTorr. The transition region is spanned by multiple pressure series due to the presence of neutral deuterium ions within the reactor. As drive power is increased, a greater number of neutrals are ionized increasing the effective plasma density and permitting a current flow to the reactor walls. It is possible to reduce this effect by choosing a sufficiently low base pressure that when the majority of the neutrals are ionized, the plasma density remains sufficiently low within the reactor as not to allow a current flow directly to the walls. As impedance increases at lower pressures, it is observed that the grid heating fraction asymptotically approaches 0.1, indicating the fundamental limitation of the grid assembly. Even though the ions behave more ideally at higher impedances, a fraction will still collide with the physical structure of the grid, causing grid heating.

Knowing the ion energies and power dissipated into the grid, the exact ion current may be calculated and used to determine secondary electron emission current. The current into the grid would consist of a sum of the electrons removed by neutralization of colliding ions and the secondary electrons generated by this collision. Approximating that all colliding ions are neutralized and that all ions have energy equal to the grid potential, the grid heating power can be used to

directly determine ion current to the grid. By subtracting this value from the total current measured at the power supply the secondary electron current may be determined. Dividing the secondary electron current by the ion current incident onto the grid surface, the number of secondary electrons emitted per ion can be determined.

The secondary electron emission rate in electrons per ion is plotted against ion energy for different pressures (Figure 4-6). In general, the graph shows an increasing trend in the number of emitted electrons as ion energy increases relating to the greater energy transferred into the metal lattice. Although the graph exhibits poor correlation between the variables, the increasing trend in secondary electron emission as a function of incident ion energy and the emission quantity of between 2 and 10 electrons per ion agrees with work done by L. N. Large et.Al. The lower correlation in these results may be attributed to device specific characteristics relating to the geometry of the device as well as effects from the presence of the plasma within the grid.

The secondary electron emission rate in electrons per ion is also plotted against grid heating power fraction. A strong correlation is observed between increasing secondary electron emission and decreasing grid heating power fraction. As secondary electron emission rates increase, more power is transferred from accelerating the ions which heat the grid during collisions, to accelerating electrons outward into the reactor shell. The accelerated electrons require a power draw but do not heat the grid thereby increasing the required Drive Power while decreasing the power dissipated into the grid, thereby reducing the grid heating power fraction as secondary electron emission rates increase. Coating the grid surface with a material exhibiting low secondary electron emission characteristics would decrease the power draw by the electron current and improve reactor efficiency

CHAPTER 6
CONCLUSION

Reduction of Thermionic Electron Emission

The cooled grid system successfully maintains a low operating temperature when subjected to intense ion bombardment, thereby eliminating thermionic electron emission. Grid systems of this type may be implemented in commercial or scientific IEC fusion devices to significantly improve reactor efficiency in operating regimens where the grid assembly is subjected to a significant heat load. The liquid cooled grid system provides a reliable means to consistently maintain low grid temperatures over a variety of operating parameters.

Use of Cooled Grid as a Diagnostic Instrument

The cooled grid assembly was successfully implemented as a diagnostic instrument to allow accurate measurements of power dissipated into the grid through ion bombardment heating. This implementation allows a direct measurement of grid heating while in non cooled grid reactor designs, the amount of grid heating can only be approximated by radiative cooling losses determined by an indirect estimation of grid temperature by pyrometric readings.

The amount of ion bombardment heating is proportional to the rate at which ions collide with the grid, directly determining the particle confinement time in the reactor. The actively cooled grid system enables measurement of relatively small changes in heat load allowing for accurate measurements of ion bombardment rate and by extension, particle confinement. The grid system would provide a direct determination of the effects of ion injectors, additional focusing grids, or additional magnetic confinement on the rate of ion grid collisions. In this manner, the grid assembly may be utilized to optimize reactor design by increasing the precision of measurements on the ion-grid collision rate used to quantify the effectiveness of novel ion confinement designs.

CHAPTER 7
FUTURE WORK

Future work on the Mark 3 reactor will consist of the full incorporation of the ECRF ion injectors as well as the addition of plasma diagnostic instrumentation. Ion current and energy analyzers will be added to allow measurement of recirculating ion current and ion energy distribution. A thompson scattering laser system will be added to allow precise measurement of ion density and temperature distributions at the plasma focus allowing for a better understanding of the density distribution at the focal point. Further control system integration will increase the logging capability and allow for faster acquisition of data.

References

De Regt, J M., R A. Engeln, F P. De Groote, J A. Van Der Mullen, and D C. Schram. "Thomson Scattering Experiments on a 100 MHz Inductively Coupled Plasma Calibrated by Raman Scattering." Rev. Sci. Instrum. 66.5 (1199): 3228-3233.

Dietrich, Carl C. Improving Particle Confinement in Inertial Electrostatic Fusion for Spacecraft Power and Propulsion. Diss. MIT, 2007. Boston: MIT, 2007.

Dougar-Jabon, V D., D V. Reznikov, and R Santos Mayorga. "Negative Hydrogen Ion ECR Source." Rev. Sci. Instrum. 63.4 (63): 2529-2531.

Hayashizaki, N, and T Hattori. "Rf Modes and Plasma Formation of Electron Cyclotron Resonance Ion Source." Rev. Sci. Instrum. 77.03A3 (2006): 1-3.

Hirsch, Robert L., and Gene A. Meeks. "Highly Efficient, Inexpensive, Medium Current Ion Source." Rev. Sci. Instrum 38.5 (1967): 621-624.

McGuire, Thomas J. Improved Lifetimes and Synchronization Behavior in Multi-Grid Inertial Electrostatic Confinement Fusion Devices. Diss. MIT, 2007. Boston: MIT, 2007.

Piefer, Gregory R. Performance of a Low-Pressure, Helicon Driven IEC 3He Fusion Device, Diss. University of Wisconsin–Madison 2006. Madison: University of Wisconsin–Madison 2006

Takamatsu, T, K Masuda, T Kyunai, H Toku, and K Yoshikawa. "Inertial Electrostatic Confinement Fusion Device with an Ion Source Using a Magnetron Discharge." NUCLEAR FUSION 46 (2006): 142-148.

Large, L. N., and W. S. Whitlock. "Secondary Electron Emission From Clean Metal Surfaces Bombarded by Fast Hydrogen Ions." PROC. PHYS. SOC. 79 (1962): 148-157.